A DNS study of turbulent mixing of two passive scalars

A. Juneja[a)] and S. B. Pope
Sibley School of Mechanical and Aerospace Engineering, Cornell University, Ithaca, New York 14853

We employ direct numerical simulations to study the mixing of two passive scalars in stationary, homogeneous, isotropic turbulence. The present work is a direct extension of that of Eswaran and Pope[1] from one scalar to two scalars and the focus is on examining the evolution states of the scalar joint probability density function (jpdf) and the conditional expectation of the scalar diffusion to motivate better models for multi-scalar mixing. The initial scalar fields are chosen to conform closely to a ''triple-delta function'' jpdf corresponding to blobs of fluid in three distinct states. The effect of the initial length scales and diffusivity of the scalars on the evolution of the jpdf and the conditional diffusion is investigated in detail as the scalars decay from their prescribed initial state. Also examined is the issue of self-similarity of the scalar jpdf at large times and the rate of decay of the scalar variance and dissipation. © *1996 American Institute of Physics.* [S1070-6631(96)03108-X]

I. INTRODUCTION

An important feature of turbulent motion is its ability to mix and to transport passive scalars at rates much higher than those due to molecular diffusion. Often, more than one scalar is involved in the mixing process. Examples of this can readily be seen in natural or engineering flows such as the dispersion of pollutants in the atmosphere, salinity and temperature fluctuations in the ocean, and the mixing of species in turbulent reactive flows. While the turbulence underlying the above flows is essentially time dependent and inhomogeneous, a detailed study of these complex flows does not highlight any one physical concept or mechanism because there are so many interacting processes at work. Indeed, it is of great interest to investigate simple flows which clearly elucidate the basic mechanisms involved in turbulent mixing without the added complications of inhomogeneity, complex flow geometries or decaying turbulence. Over the last couple of decades, direct numerical simulations (DNS) of the Navier-Stokes equations have emerged as a leading research tool for examining the physics of turbulence at moderate Reynolds numbers because of their unique ability to provide fully resolved spatio-temporal evolution of the flow fields without any modeling or approximations. Consequently, the present work employs DNS to study the mixing of two decaying scalar fields with a prescribed initial joint probability density function (jpdf) in statistically stationary, homogeneous, isotropic turbulence.

A significant amount of experimental and computational effort has been exerted to study the mixing of a single passive scalar in turbulent flows. A number of researchers have studied the evolution of one-point and two-point quantities of scalar fields in grid turbulence (see, e.g., Refs. 2 and 3). Laser Induced Flouresence (LIF) techniques have been used to obtain and study images of instantaneous scalar fields in turbulent flows[4,5] and Dahm *et al.*[6] have developed a method for acquiring a sequence of planar LIF images sweeping a volume to get four-dimensional experimental data on scalar mixing. On the other hand, Eswaran and Pope[1] employed DNS to examine the evolution of the probability density function of a single scalar from an initial double-delta function distribution, while Kerr[7] used DNS to examine the small scale structure of the passive scalar. Blaisdell *et al.*[8] have carried out simulations to assess the effects of compressibility on the mixing process, and Pumir[9] has studied the case with a mean scalar gradient. Chasnov[10] also used DNS to present results for the similarity states of a passive scalar field transported by isotropic and buoyancy generated turbulence. Theoretical approaches which have been applied to the mixing of a single scalar with some success include probability density function (pdf) methods,[11] mapping closures[12] and the linear eddy model.[13]

In contrast, data on the mixing of multiple scalars is relatively scarce. Sirivat and Warhaft[14] measured the correlation between passive helium and temperature measurements in grid generated turbulence. Warhaft[15] also developed an inference technique to study the covariance of thermal fluctuations introduced in decaying turbulence at different locations. Yeung and Pope[16] employed DNS to examine the differential diffusion of two scalars having different diffusivities starting from an identical field for the two scalars, while experimental studies of differential diffusion have been reported by Saylor[17] among others. The extension of the theoretical approaches to multi-scalar mixing is far from straightforward, and is further hampered by the lack of experimental or numerical data which can aid in model comparison and development.

Research on turbulent mixing processes is especially instructive in turbulent-reactive flow problems. Here, in the limit of fast chemistry, one of the vital factors limiting the rate of reaction is the mixing of initially segregated scalar fields at the smallest scales at which the chemical reaction takes place. Pdf formulations have had considerable success in modeling reactive flow problems.[11] These methods have the important advantage of treating the effects of advection and the nonlinear reaction rates exactly: however the process of molecular mixing needs to be modeled. We consider non-

---
[a)]Present address: Department of Mechanical Engineering, The Pennsylvania State University, University Park, Pennsylvania 16802.

TABLE I. Summary of specified quantities for initial velocity fields.

Vel. field	R92	R48
N	192	96
ν	0.008	0.025
K_F	$2\sqrt{2}$	$2\sqrt{2}$
$Re*$	14.4	14.4
T_F^*	0.15	0.15
C_N	0.8	0.8

reactive scalar fields $\phi_\alpha(\mathbf{x},t), \alpha=1,2$, which evolve by

$$\frac{\partial \phi_\alpha}{\partial t} + u_i \frac{\partial \phi_\alpha}{\partial x_i} = D_{(\alpha)} \nabla^2 \phi_\alpha, \qquad (1)$$

where $\mathbf{u}(\mathbf{x},t)$ is the velocity and $D_{(\alpha)}$ is the diffusivity of the scalar α. (Suffixes in parentheses are excluded from the summation convention.) For the statistically homogeneous case under consideration, the one-point one-time joint probability density function (jpdf) of the two scalars is denoted by $P(\boldsymbol{\psi},t)$, where $\boldsymbol{\psi}=(\psi_1,\psi_2)$ are the sample space variables corresponding to $\boldsymbol{\phi}=(\phi_1,\phi_2)$. This jpdf evolves by[11]

$$\frac{\partial P(\boldsymbol{\psi},t)}{\partial t} = -\frac{\partial}{\partial \psi_\alpha}[P(\boldsymbol{\psi},t)\gamma_\alpha(\boldsymbol{\psi},t)], \qquad (2)$$

where the conditional diffusion $\boldsymbol{\gamma}(\boldsymbol{\psi},t)$ is defined to be the conditional expectation,

$$\gamma_\alpha(\boldsymbol{\psi},t) = \langle D_{(\alpha)}\nabla^2 \phi_\alpha | \boldsymbol{\phi}(\mathbf{x},t)=\boldsymbol{\psi}\rangle. \qquad (3)$$

In the present work, we examine the evolution of the scalar jpdf P and the conditional diffusion $\boldsymbol{\gamma}$ for the mixing of two scalars starting from a prescribed initial state (triple-delta function jpdf). The work is in essence an extension of that presented in Eswaran and Pope (hereafter EP) and it is hoped that the present results will provide the necessary impetus for the development of better mixing models for the multi-scalar case.

A parallel implementation of Rogallo's pseudospectral algorithm[18] for the IBM SP2 is used to carry out direct numerical simulations of the governing equations in a cubic domain with periodic boundary conditions. The low wavenumber modes are forced using the scheme described in Eswaran and Pope[19] to preserve statistical stationarity in the velocity fields. The scalar fields are allowed to decay from their prescribed initial state and we examine the evolution of the scalar jpdf and the conditional diffusion in detail. The

TABLE II. Summary of derived quantities for initial velocity fields.

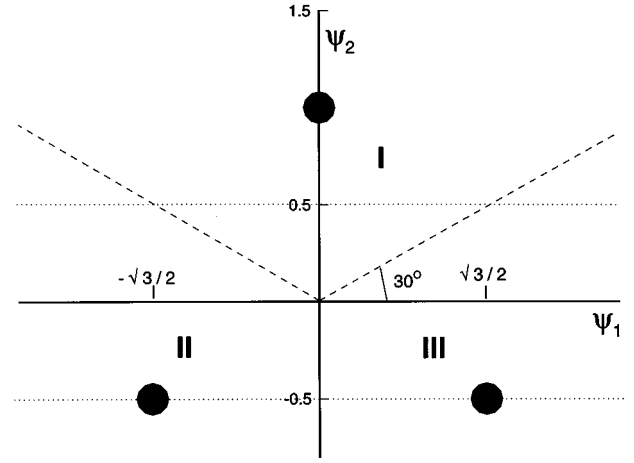| Vel. field	R92	R48
u	2.06	2.16
$k_0 l$	1.10	1.05
$k_0 \lambda$	0.35	0.51
$k_0 \eta$	0.02	0.04
$k_{max} \eta$	1.65	1.78
$D*$	0.49	0.49
T	0.52	0.50
τ_η / T	0.08	0.14
Re_λ	92.4	48.6

FIG. 1. A schematic for the initialization of the scalar fields. The composition plane represented by ψ_1-ψ_2 is divided into three sectors by the two dashed lines and the negative ψ_2 axis. The filled circles correspond to the three initial states for the two scalar fields. (The evolution of the conditional diffusion in Fig. 5 is shown along the two axes and the two dotted lines.)

effect of varying the initial length scales and the Prandtl number of the two scalars on the mixing process is investigated. Also examined is the tendency of the scalar jpdf to reach a statistically self-similar state at large times as well as the rate of decay of scalar variance and the mean scalar dissipation rate. Nearly all the simulations were carried out on a 192^3 grid at a Taylor-scale Reynolds number of $Re_\lambda=92$, excepting a few requiring the extraction of statistics at large times which were performed on a smaller 96^3 grid at a Taylor-scale Reynolds number of $Re_\lambda=48$ in order to keep the overall computational costs low. This also gave an opportunity to qualitatively compare the mixing process at different Reynolds numbers.

The remainder of the paper is organized as follows. In Sec. II we provide a brief overview of the simulations including the numerical method, parallel implementation and the input flow conditions. In Sec. III we describe the method for initializing the two scalar fields. The results from the simulations are presented in Sec. IV. We conclude the paper with a summary in Sec. V.

II. OVERVIEW OF THE SIMULATIONS

A. The numerical method

For incompressible flows, the equations governing the evolution of the velocity and scalar fields can be written as

TABLE III. Summary of input parameters for scalar fields.

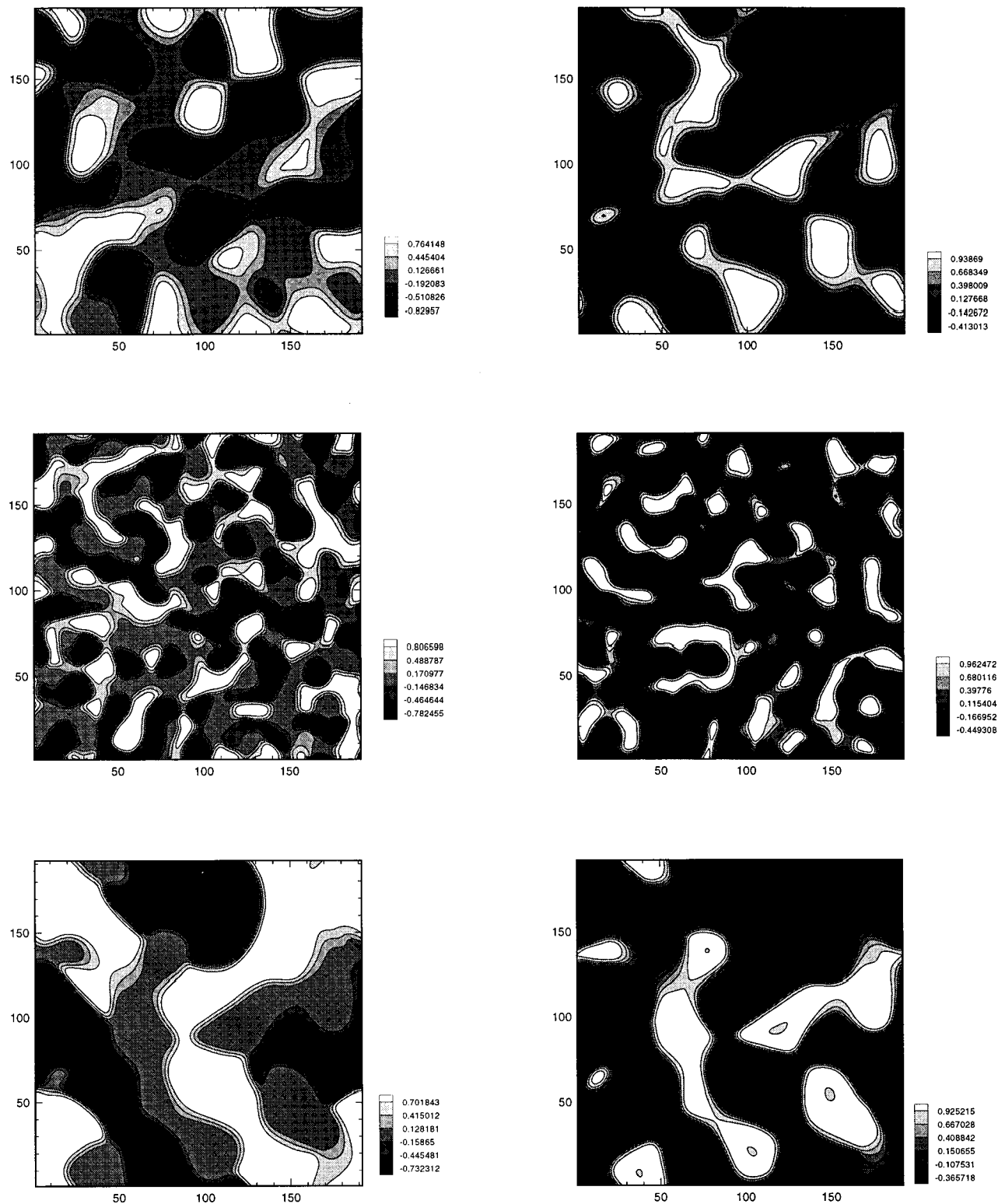| Scalar field	A	B	C	D	E
$(k_s/k_0)_1$	4	8	2	2	4
$(k_s/k_0)_2$	4	8	2	4	4
Pr_1	0.7	0.7	0.7	0.7	0.7
Pr_2	0.7	0.7	0.7	0.7	0.35
l_{ϕ_1}	0.38	0.16	0.62	0.62	0.38
l_{ϕ_2}	0.37	0.18	0.58	0.40	0.37
$\langle \phi_1 \phi_2 \rangle$	−0.0006	0.0025	0.001	−0.009	−0.0006

A. Juneja and S. B. Pope

FIG. 2. Contour plots of a planar slice through the initial scalar fields, $\phi_1(\mathbf{x},0)$ (left column) and $\phi_2(\mathbf{x},0)$ (right column) for cases A (top row), B (middle row) and D (bottom row).

$$\frac{\partial u_i}{\partial x_i} = 0, \tag{4}$$

$$\frac{\partial u_i}{\partial t} + u_j \frac{\partial u_i}{\partial x_j} = -\frac{1}{\rho}\frac{\partial p}{\partial x_i} + \nu \frac{\partial^2 u_i}{\partial x_j \partial x_j}, \tag{5}$$

$$\frac{\partial \phi_\alpha}{\partial t} + u_j \frac{\partial \phi_\alpha}{\partial x_j} = D_{(\alpha)} \frac{\partial^2 \phi_\alpha}{\partial x_j \partial x_j}, \tag{6}$$

where u_i is the component of the velocity in the ith direction. A modified version of the pseudo-spectral method developed
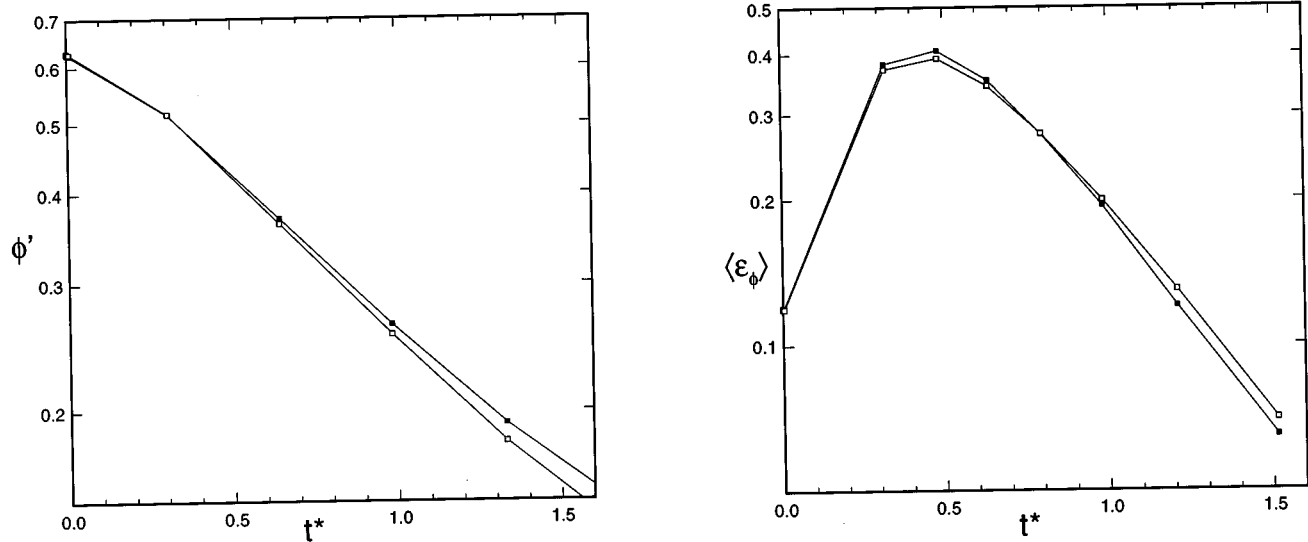
Phys. Fluids, Vol. 8, No. 8, August 1996

A. Juneja and S. B. Pope   2163

FIG. 3. The evolution of the scalar r.m.s (ϕ') and the mean scalar dissipation ($\langle \epsilon_\phi \rangle$) from the R92A simulations. t^* represents the time normalized by the eddy-turnover time T. The filled symbols correspond to ϕ_1 while the hollow symbols are for ϕ_2.

by Rogallo[18] for homogeneous turbulent flows was used to solve the above equations numerically on a uniform three-dimensional grid. In physical space, this corresponds to a cube of side $L=2\pi$ with the N^3 grid points located at $x=(l_1\Delta, l_2\Delta, l_3\Delta)$, where l_1, l_2 and l_3 are integers between 0 and $N-1$ and the grid spacing Δ is equal to L/N. The nodes in wavenumber space are located at $k=(m_1, m_2, m_3)$ where m_1, m_2 and m_3 are integers between $1-N/2$ and $N/2$. (The smallest wavenumber is $k_0=1$ owing to L being equal to 2π.) The use of Fourier representation imposes periodic boundary conditions on the velocity and scalar fields.

Briefly, the pseudo-spectral method solves the above equations in spectral space because of the associated higher accuracy in computing the spatial derivatives. However, the bilinear products required for the convective terms are computed in physical space to avoid the costly operation of convolutions in Fourier space. The aliasing errors introduced by the transformation of these products back to Fourier space are greatly reduced by a combination of phase shifts and truncation. The viscous terms are treated exactly and are thus eliminated as a stability constraint. The time advance of the Fourier transformed equations is performed using an explicit second-order Runge-Kutta method.

The numerical simulations are forced using the method described in Eswaran and Pope.[19] It consists of the addition of a random term to the velocity time derivative in Fourier space, at every time step, for each non-zero wavenumber node k lying within the spherical shell of radius K_F. The random term is determined using a combination of independent Uhlenbeck-Ornstein processes. The forcing scheme introduces three nondimensional quantities in the form of a forcing Reynolds number Re^*, a forcing time scale T^* and the ratio K_F/k_0 (see Ref. 19 for details). Each of these parameters is kept constant for all the simulations presented herein.

Numerical accuracy depends on both the spatial and the temporal resolution. The former requires that the smallest dynamically significant scales of motion characterized by the Kolmogorov length scale η be well resolved by the physical grid. It is customary to characterize the spatial resolution of a simulation by the dimensionless parameter $k_{max}\eta$ where k_{max} is the highest resolvable wavenumber of the simulation. It has been suggested that a value of $k_{max}\eta=1.0$ is adequate for low-order velocity statistics, but a value of at least 1.5 is needed for higher-order quantities such as the dissipation and derivative statistics.[20] In order to determine the resolution requirements for the evolution of the scalar field, we carried out test simulations with one passive scalar (Prandtl number, $Pr=0.7$) on 64^3, 96^3 and 128^3 grids at a Taylor-scale Reynolds number of $Re_\lambda=50$ corresponding to $k_{max}\eta$ being approximately equal to 1.1, 1.6 and 2.2, respectively. It was found that the evolution of $\langle \nabla^2\phi \rangle$ and $\langle \nabla^4\phi \rangle$ was very similar for the two finer grids in contrast to the coarser grid. Hence we concluded that $k_{max}\eta \geq 1.5$ provides sufficient resolution for the accurate calculation of higher-order scalar statistics as well. The accuracy of the time integration, on the other hand, is determined by the Courant number defined as $C_N=\Sigma_{i=1}^3 (|u_i|/\Delta)_{max}\Delta t$, where Δt is the size of the time step. The Courant number was kept constant at a value of $C_N=0.8$ in our simulations in accordance with earlier suggestions[19] that it should be less than one for time stepping errors to be negligibly small.

B. Parallel implementation

The simulations were carried out on the 512-node IBM SP2 at the Cornell Theory Center. The programming model employed was the single-program multiple data (SPMD) approach where the same version of the program runs on all nodes. However, the work arrays are distributed across processors so that each node performs the same operation on its
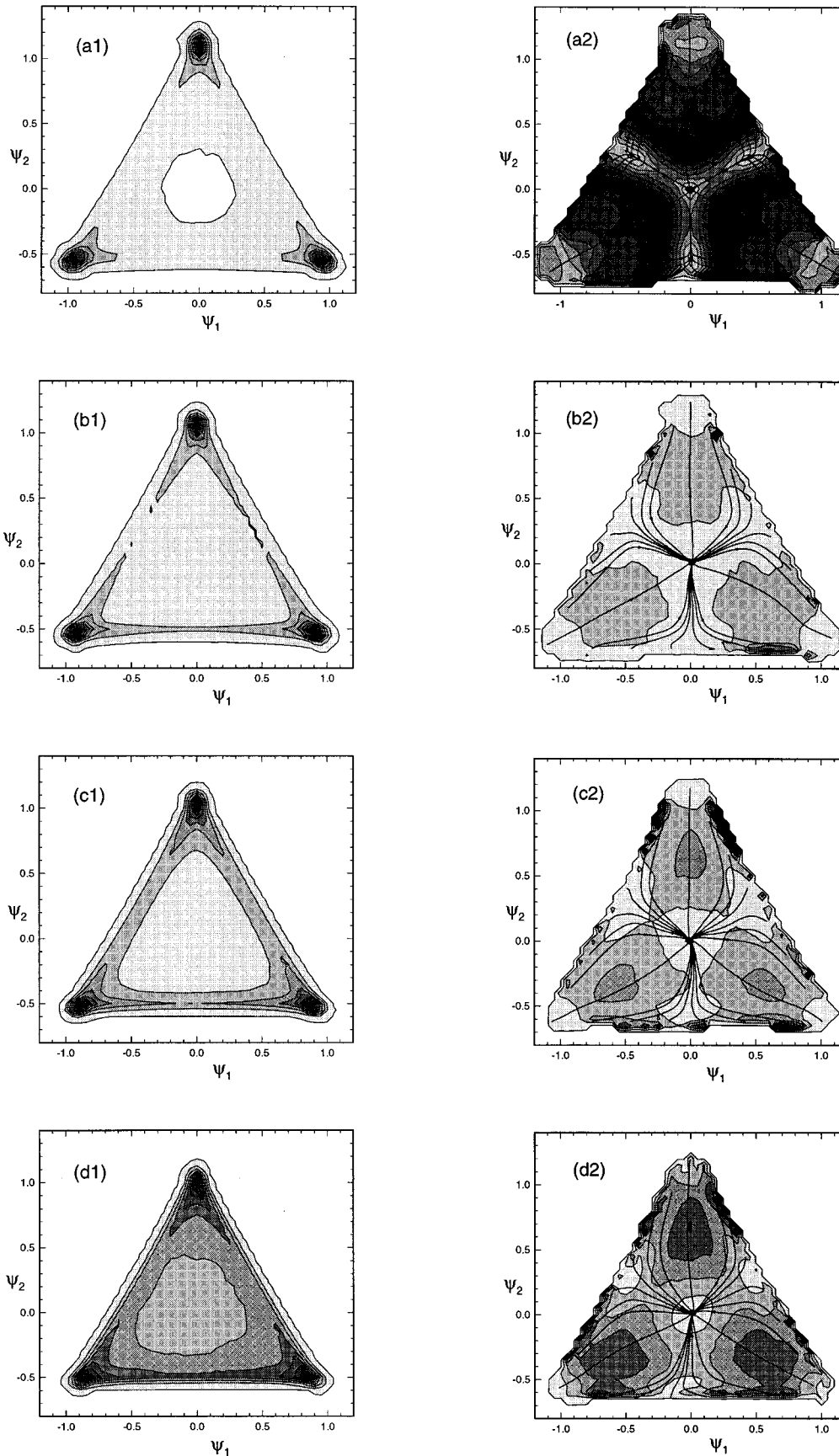
A. Juneja and S. B. Pope

FIG. 4. The evolution states of the scalar jpdf, P, (a1-j1) and the corresponding conditional diffusion, γ, (a2-j2) from the R92A simulations. The plots are shown at fixed values of Φ corresponding to 1.0 for (a), 0.9 for (b), 0.8 for (c), 0.7 for (d), 0.6 for (e), 0.5 for (f), 0.4 for (g), 0.3 for (h), 0.2 for (i) and 0.1 for (j), respectively. Both P and $|\gamma|$ have been normalized by their respective maximum values at that time in each sub-plot, so that the greyscale in the contour plots corresponds to eight equispaced shades between 0 (white) and 1 (black).
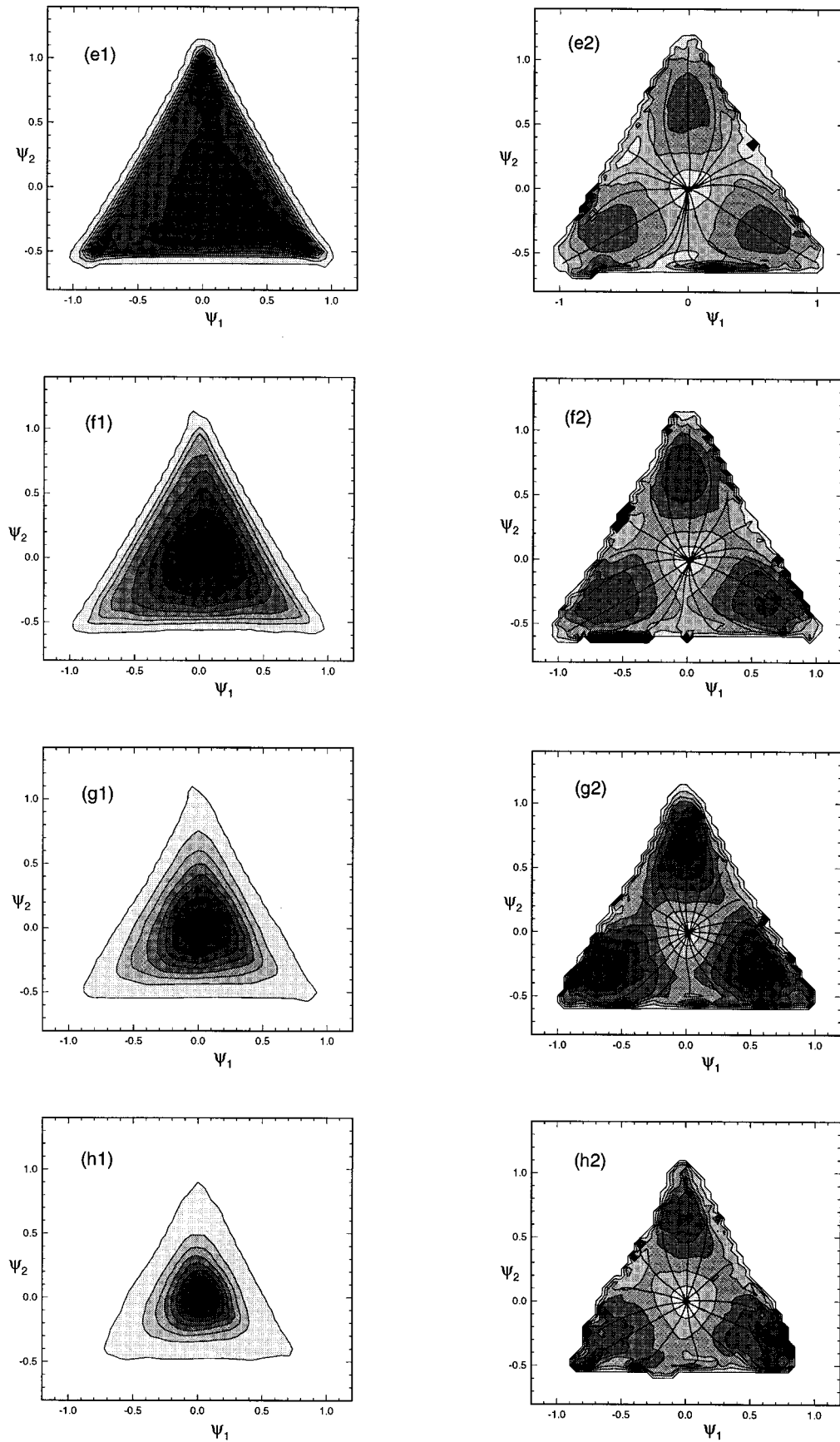
Phys. Fluids, Vol. 8, No. 8, August 1996

A. Juneja and S. B. Pope   2165
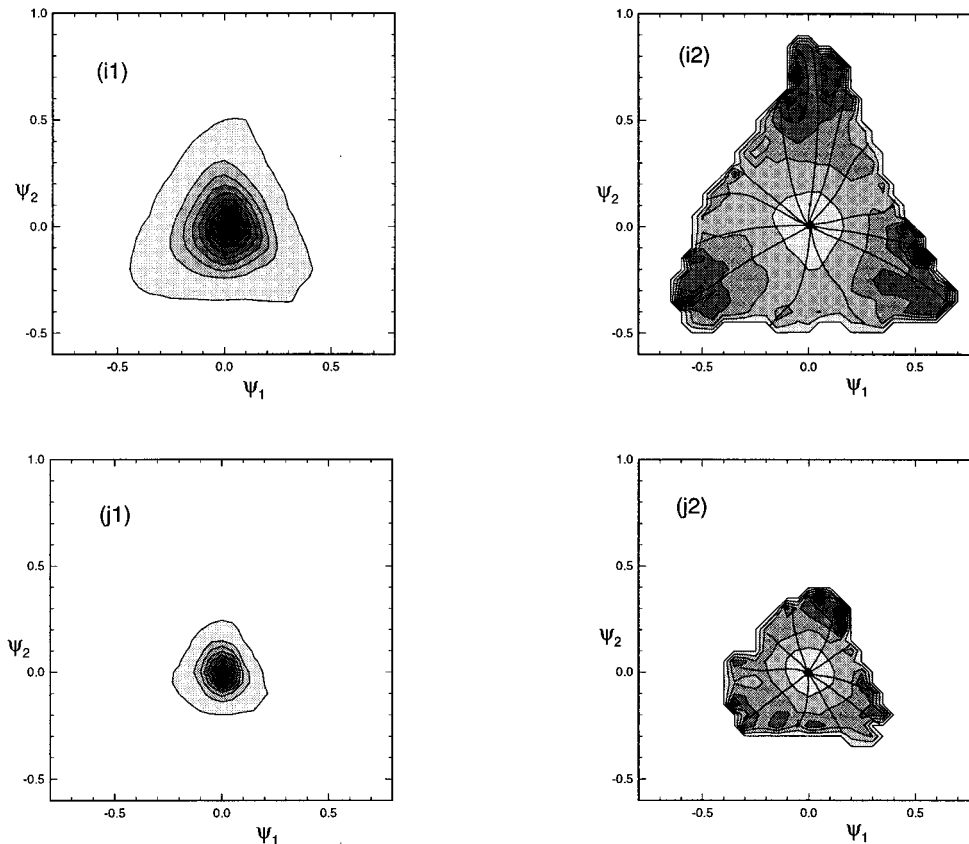
FIG. 4. (*Continued.*)

FIG. 4. (*Continued.*)

section of arrays. Node specific computations can also be carried out by ascertaining the node identification number. Such a programming model is inherently suited to the distributed-memory message-passing parallel architecture of the SP2, as the associated data parallelism allows the solution of a larger problem (more grid points) on extra processors without any appreciable degradation of the parallel efficiency. [Parallel efficiency is defined as the ratio of observed speedup in the execution time of the code on P processors to the ideal speedup (P).]

The bulk of the computational effort in a pseudo-spectral algorithm involves the use of Fast Fourier Transforms (FFT) to transform the data interchangeably between the physical and the Fourier space. Consequently, we performed several tests to determine the best way of distributing data among processors which would yield the highest parallel efficiency for the FFT computations. Our conclusion was the same as that arrived at by Yeung and Moseley[21] namely that the data should be stored in planar slabs among processors with some transfer of data involved to compute the FFT in the third direction as follows: while in physical space, the data are stored in y-slabs (i.e., partitions of data in which the nodes have complete x-z planes of data for a particular y extent) and the x and the z transform of the data is computed. Then using a collective communications procedure, the data are transferred across processors such that each node now contains z-slabs of data, and the y transform is computed to

complete the transformation to Fourier space. The inverse procedure is followed for transforming the data from Fourier to physical space. For all other computations in the DNS code requiring the transfer of data (such as the computation of the spectra, forming the histograms for the jpdf's), each processor first does the computation on its share of data, and the results are then binned together at the master node for output. This can be achieved with relatively high parallel efficiencies of greater than 90% since the amount of data transfer across processors is small. As for the complete DNS code, for simulations on a 192^3 grid on 32 processors, we consistently achieved parallel efficiencies of greater than 75% based on the wallclock time required for the execution.

C. Flow field characteristics

Two grid sizes and Reynolds numbers are used in the simulations. The larger grid calculations ($N = 192$) are labeled R92 (indicating $Re_\lambda = 92$), while the smaller grid calculations ($N = 96$) are labeled R48 (i.e., $Re_\lambda = 48$). The input parameters are given in Table I. For each case a presimulation is performed in which, starting from random initial conditions, the velocity fields are advanced in time (for about six eddy-turnover times) until a statistically stationary state is achieved. The resulting velocity fields are then stored and used as initial conditions for the mixing simulations. The characteristics of the turbulence in the statistically stationary

Phys. Fluids, Vol. 8, No. 8, August 1996

A. Juneja and S. B. Pope   2167
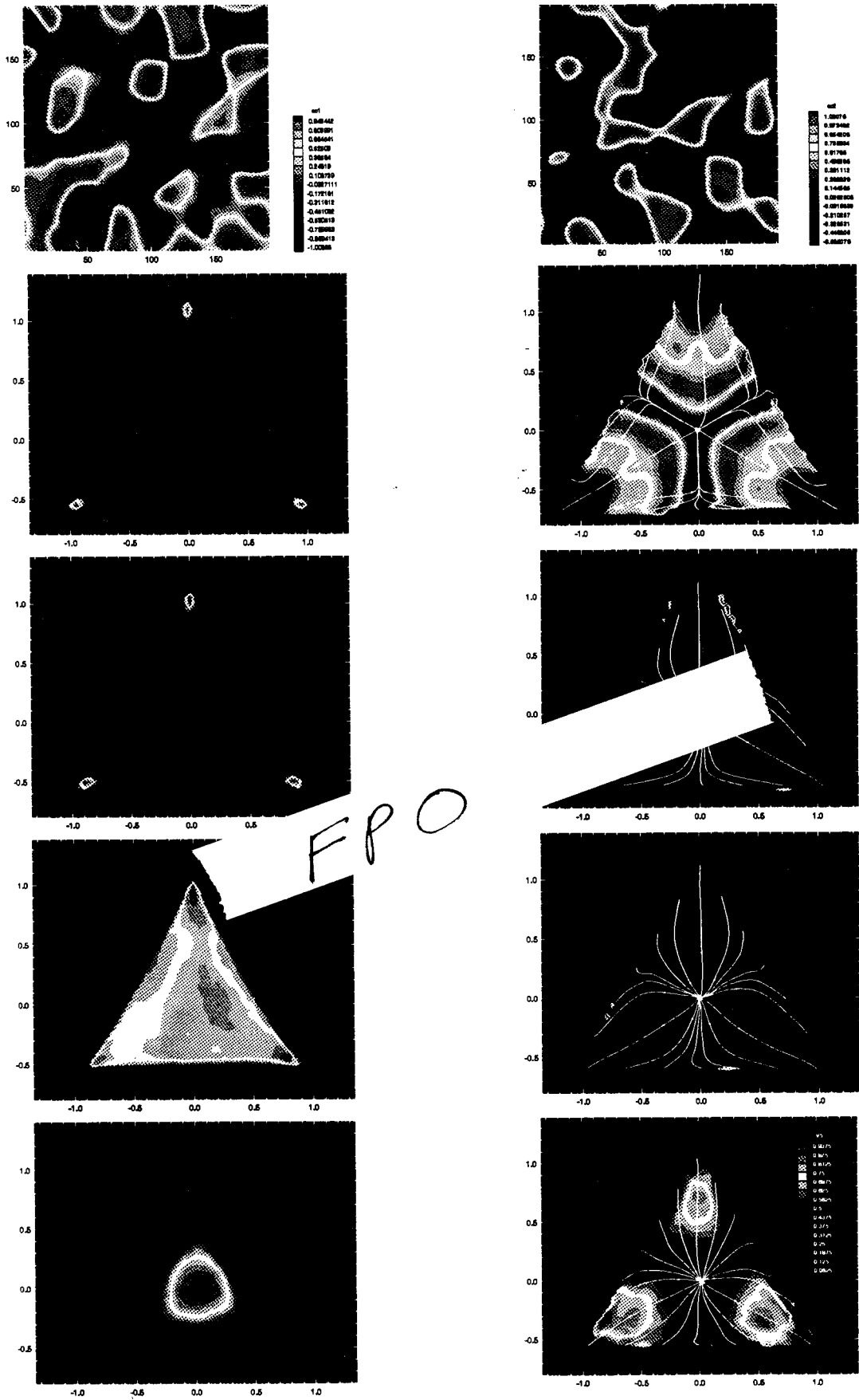
Color Plate 1: Results from the R92A simulations. The top row shows an arbitrary planar slice through the initial scalar fields, ϕ_1 (left) and ϕ_2 (right), while the second through fifth rows show the evolution states of the scalar jpdf (left) and conditional diffusion (right) at $\Phi=1.0$, 0.8, 0.6, and 0.4, respectively. (See also the caption for Fig. 4.)
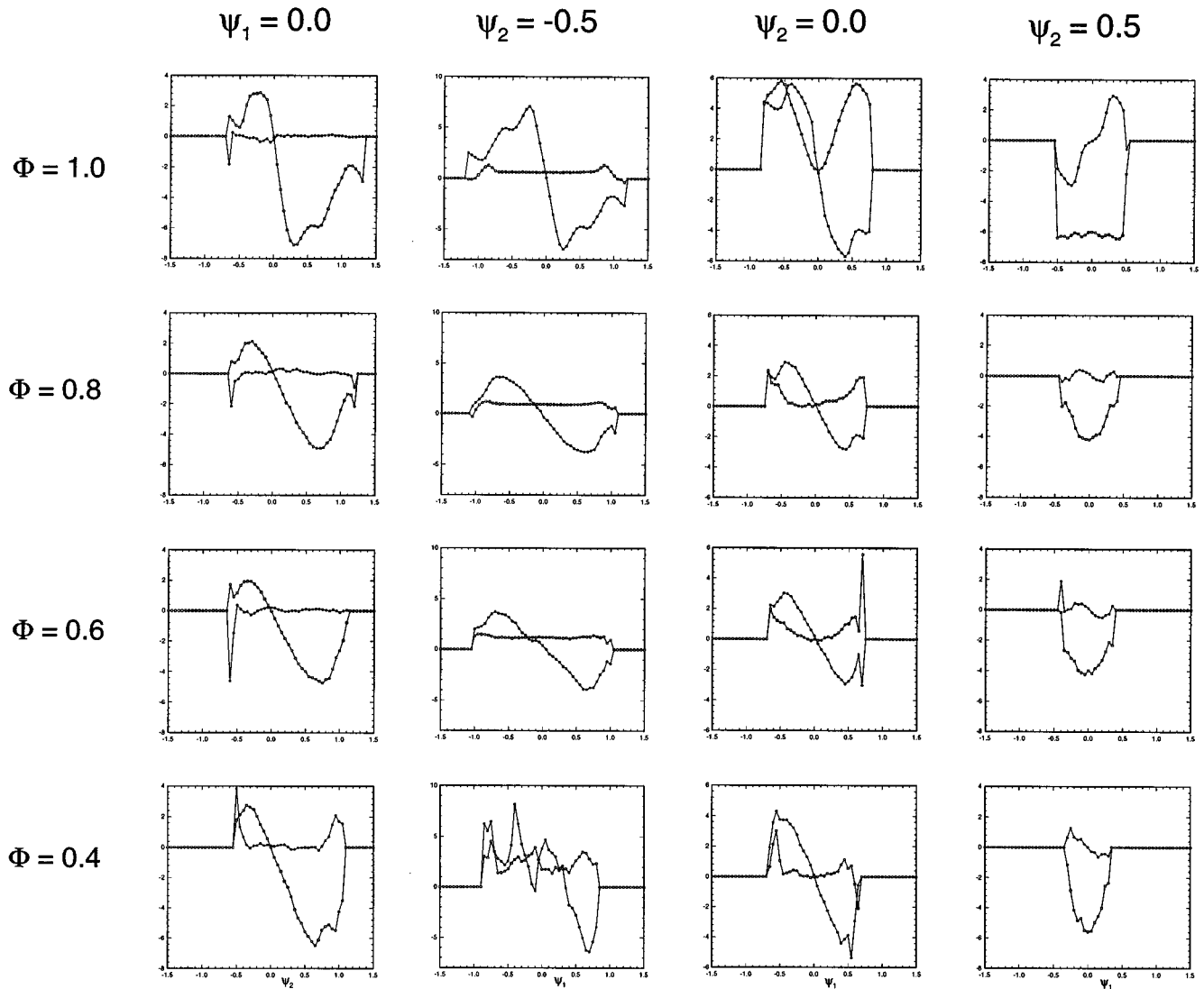
2168   Phys. Fluids, Vol. 8, No. 8, August 1996

A. Juneja and S. B. Pope

FIG. 5. The evolution of the normalized values of γ_1 and γ_2 from the R92A simulations. Each column represents a fixed line in the composition plane and each row a fixed time from the simulations. Column 1 corresponds to the $\psi_1=0$ line, column 2 to the $\psi_2=-0.5$ line, column 3 to $\psi_2=0.0$ line, and column 4 to $\psi_2=0.5$ line (see Fig. 1). The values of γ_1 (filled squares) and γ_2 (hollow squares) along these lines are plotted at $\Phi=1.0$ (row 1), $\Phi=0.8$ (row 2), $\Phi=0.6$ (row 3), and $\Phi=0.4$ (row 4), respectively.

state are given in Table II. The root mean square velocity (averaged over the three components) is denoted by u. The three length scales characterizing the energy-containing scales, the dissipation scales and the mixed energy-dissipation scales, respectively, are the integral scale,

$$l=\frac{\pi}{2u^2}\int_0^{k_{max}} k^{-1}E(k)dk; \tag{7}$$

the Kolmogorov microscale,

$$\eta=(\nu^3/\epsilon)^{1/4}; \tag{8}$$

and the Taylor microscale,

$$\lambda=\frac{1}{3}\sum_{i=1}^{3}\left[\frac{u_{(i)}^2}{\langle(\partial u_{(i)}/\partial x_{(i)})^2\rangle}\right]^{1/2}, \tag{9}$$

where $E(k)$ is the energy spectrum function at scalar wavenumber $k=(\mathbf{k}\cdot\mathbf{k})^{1/2}$, and ϵ is the volume averaged energy dissipation rate and D^* is its non-dimensionalized value $(D^*\equiv\epsilon/u^3k_0)$. The time scale of the energy-containing eddies is the eddy-turnover time $T=l/u$ and the time scale of the dissipation range eddies is the Kolmogorov timescale $\tau_\eta=(\nu/\epsilon)^{1/2}$. The Reynolds number characterizing the simulations is $Re_\lambda=u\lambda/\nu$.

III. INITIAL SCALAR FIELDS

Eswaran and Pope[1] studied the mixing of a single scalar (ϕ_1) with an initial (approximate) double-delta-function pdf corresponding to blobs of fluid in two distinct states, $\phi_1\approx-1$ and $\phi_1\approx1$. Here we extend these ideas to study the mixing of two scalars with an initial (approximate) triple-
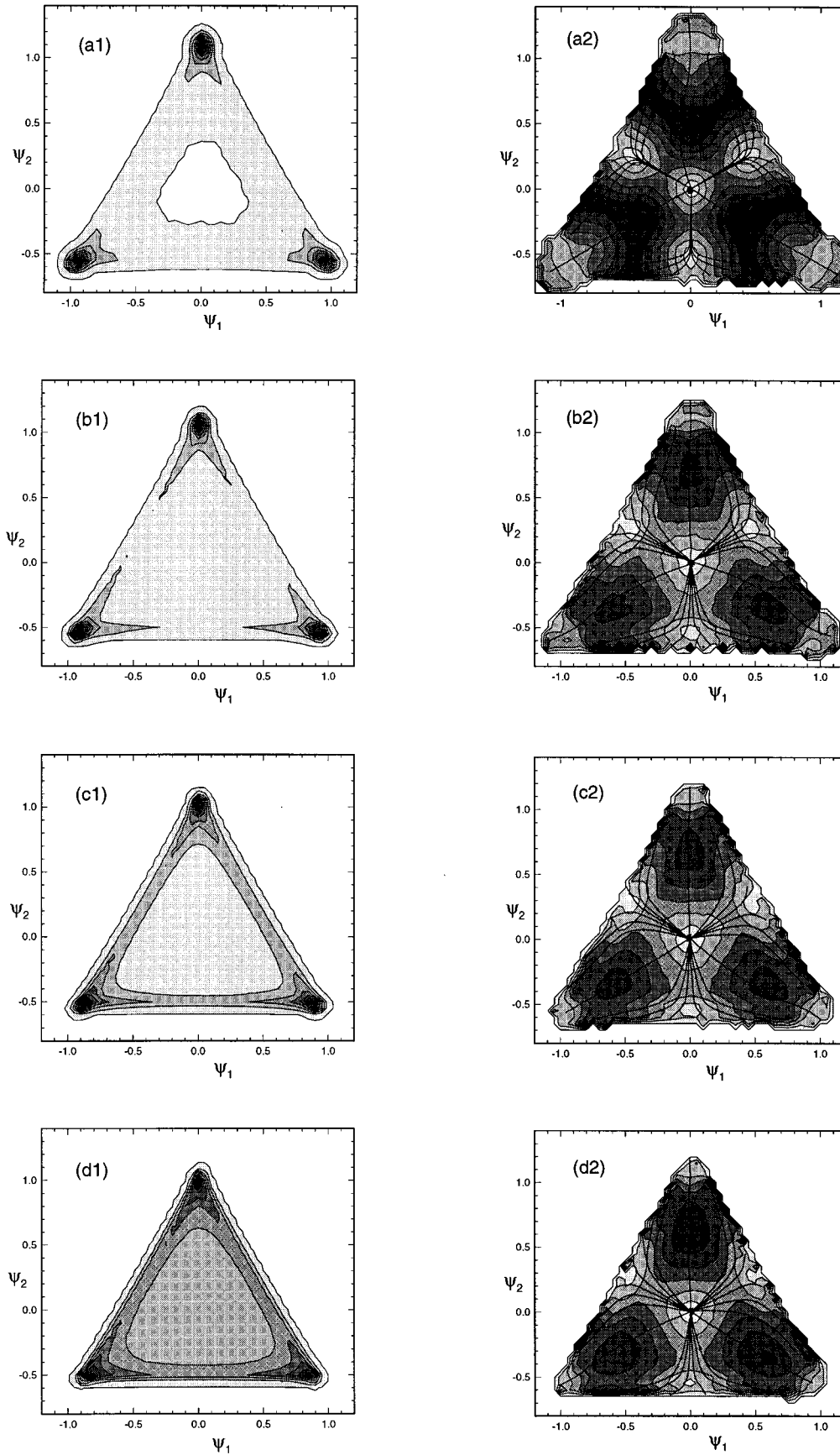
Phys. Fluids, Vol. 8, No. 8, August 1996

A. Juneja and S. B. Pope   2169

FIG. 6. Same as Fig. 4, but for R92B simulations.
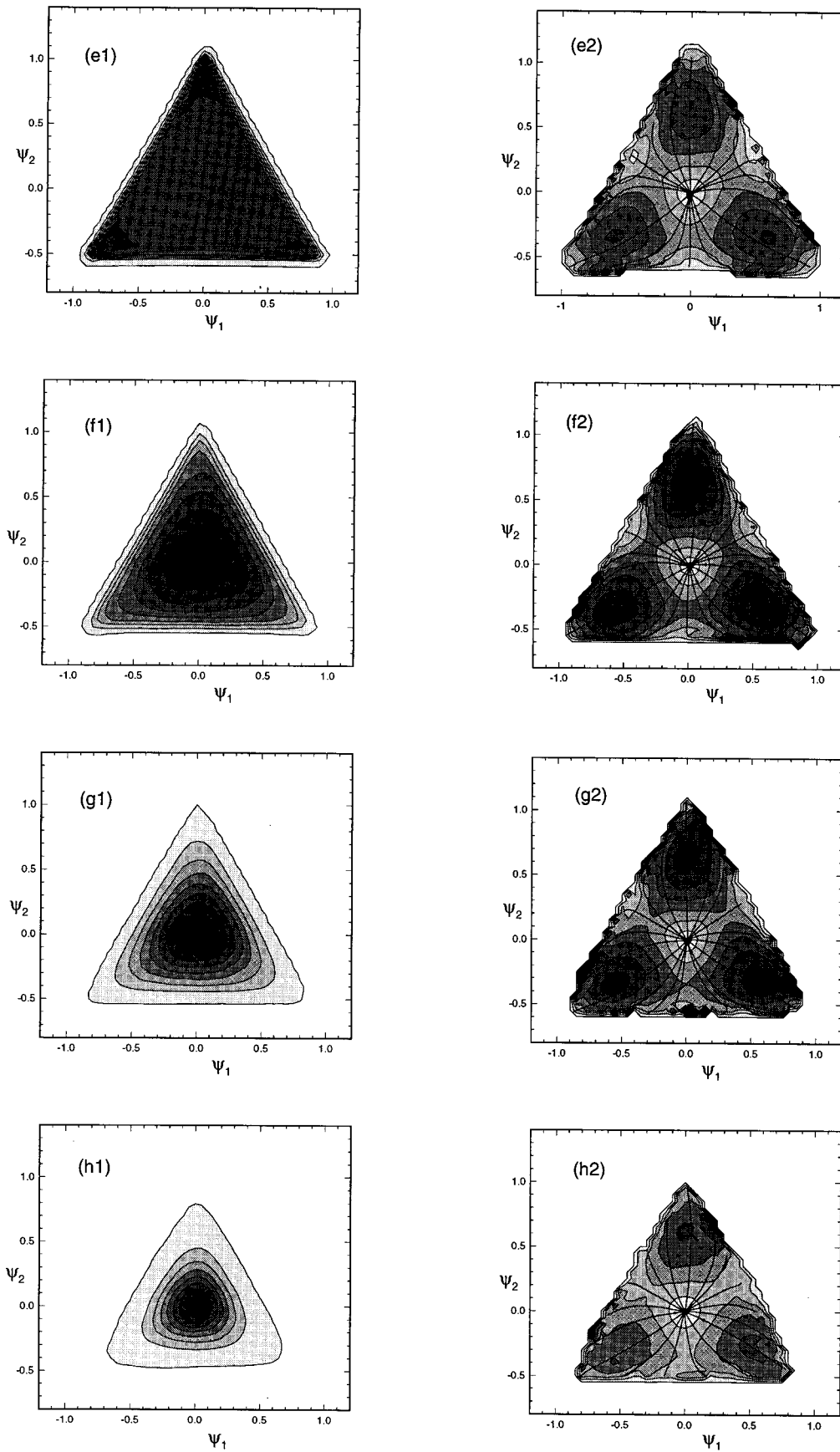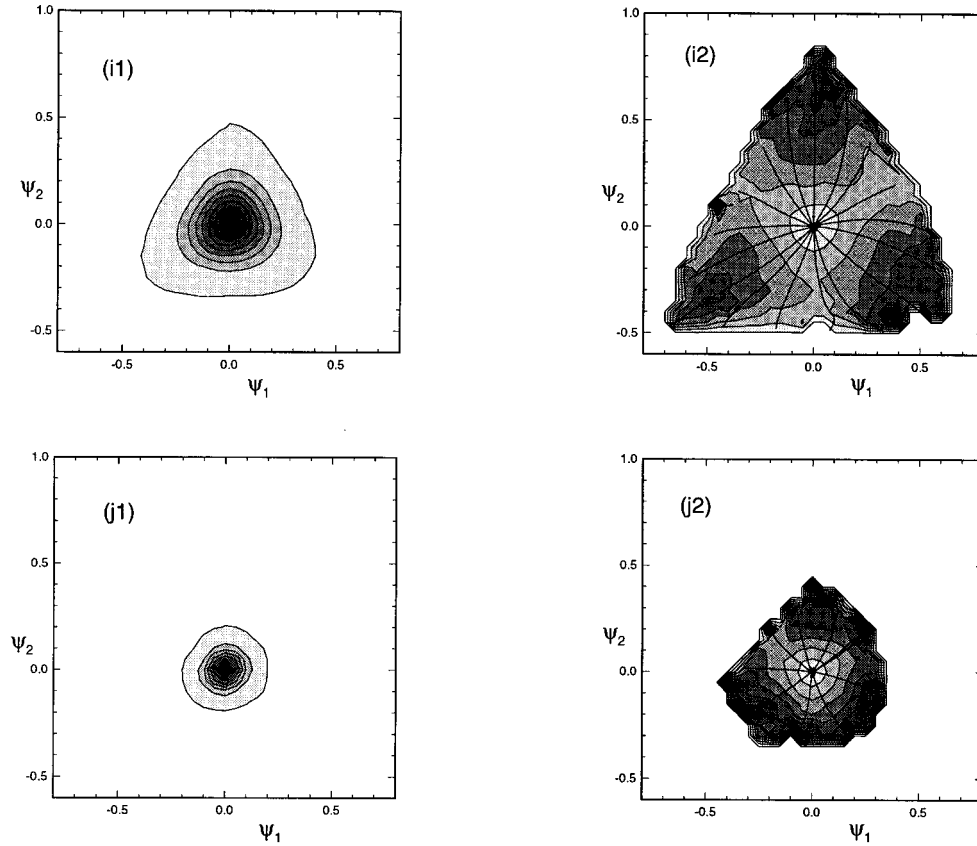
A. Juneja and S. B. Pope

FIG. 6. (*Continued.*)

FIG. 6. (*Continued.*)

delta-function jpdf, corresponding to blobs of fluids of three distinct states. As depicted in Fig. 1, in the ψ_1-ψ_2 sample space, the three states correspond to the vertices of an equilateral triangle, and lie on the unit circle around the origin. Each initial state has equal probability, so that the means $\langle \phi_1 \rangle$ and $\langle \phi_2 \rangle$ are zero. This ensures that in the composition space the initial state has a three-way symmetry, and even though the two scalar fields are not interchangeable, a 120° rotation maps one onto the other. The initialization scheme employed is analogous to the procedure followed in EP such that the initial fields $[\phi_1(\mathbf{x},0), \phi_2(\mathbf{x},0)]$ conform closely to a triple-delta function jpdf, are resolved by the grid, and have a specified length scale. This is accomplished by a three-step procedure.

In the first step, two independent fields are defined in Fourier space with random phases for each of the Fourier coefficients. The respective amplitudes are determined such that the resultant scalar energy spectrum function is given by a specified function $f_\phi(k)$. This can be equivalently stated as follows:

$$\phi_{1,2}(\mathbf{k},0) = \left[\frac{f_\phi(k)}{4\pi k^2} \right] \exp[2\pi i\, \theta(\mathbf{k})], \qquad (10)$$

where k is the magnitude of the wavenumber $\mathbf{k}$ and $\theta(\mathbf{k})$ is a uniformly distributed random number between 0 and 1 (independent of the wavenumber $\mathbf{k}$). The function $f_\phi(k)$ is chosen to be a ''top hat'' function of width k_0 and centered on a selected wavenumber k_s, i.e.,

$$f_\phi(k) = \begin{cases} 1, & \text{if } k_s - k_0/2 \leqslant k \leqslant k_s + k_0/2, \\ 0, & \text{otherwise.} \end{cases} \qquad (11)$$

As shown in EP, the parameter k_s/k_0 essentially determines the integral length scale of the scalar fields. Higher values of k_s/k_0 yield smaller length scales for the scalar fields and vice versa. Further, the value of k_s/k_0 for the first scalar [hereafter $(k_s/k_0)_1$] can be different from the value of k_s/k_0 for the second scalar [hereafter $(k_s/k_0)_2$].

In the second step, the two scalar fields are transformed to physical space and the composition plane ψ_1-ψ_2 is divided into the three sectors shown in Fig. 1. If at point $\mathbf{x}$, the scalar values $\phi_1(\mathbf{x}), \phi_2(\mathbf{x})$ (obtained from the first step) lie in the first sector of the ψ_1-ψ_2 composition plane, then the values are reset to the first state, i.e., $(\phi_1(\mathbf{x}), \phi_2(\mathbf{x})) = (0,1)$. Similarly, if $\boldsymbol{\phi}(\mathbf{x})$ lies in the second or third sector, it is reset to $(-\sqrt{3}/2, -1/2)$ or $(\sqrt{3}/2, -1/2)$, respectively. This operation yields the desired joint probability density function for the two scalar fields, but causes the scalar value to change abruptly between adjacent nodes, thereby causing significant high-wavenumber components in the scalar fields which are poorly resolved in the simulations.

The third and final step in the initialization scheme therefore seeks to smooth out the scalar fields just enough so that they are well resolved for the given grid size of the simulation. This is achieved by transforming the fields defined at the end of the second step back to Fourier space and then multiplying them by a filter function $F(\mathbf{k})$, defined by
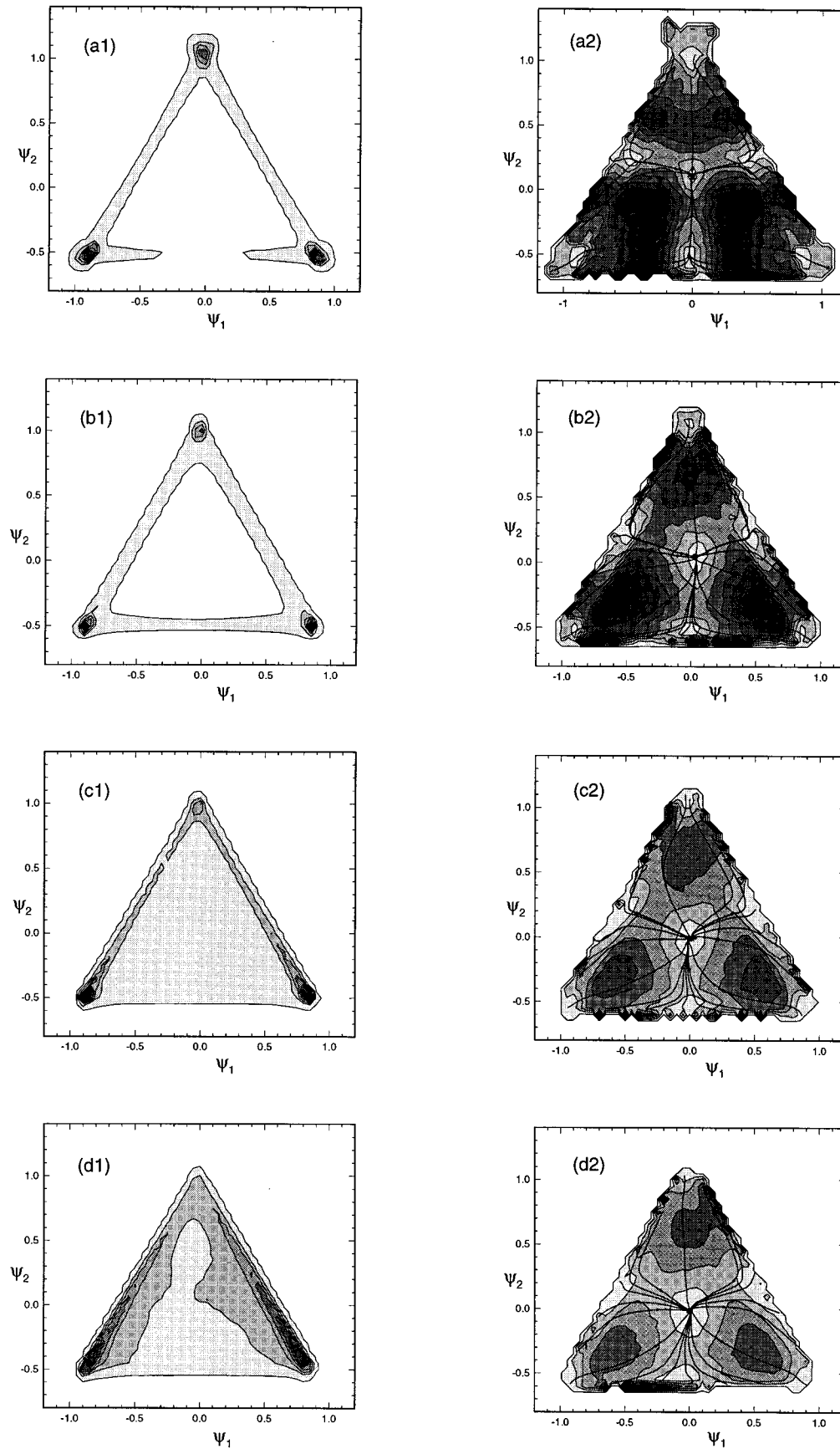
A. Juneja and S. B. Pope

FIG. 7. Same as Fig. 4, but for R92D simulations (the plots at $\Phi = 0.2$ and 0.1 are not shown).

Phys. Fluids, Vol. 8, No. 8, August 1996

A. Juneja and S. B. Pope   2173

FIG. 7. (*Continued.*)

A. Juneja and S. B. Pope
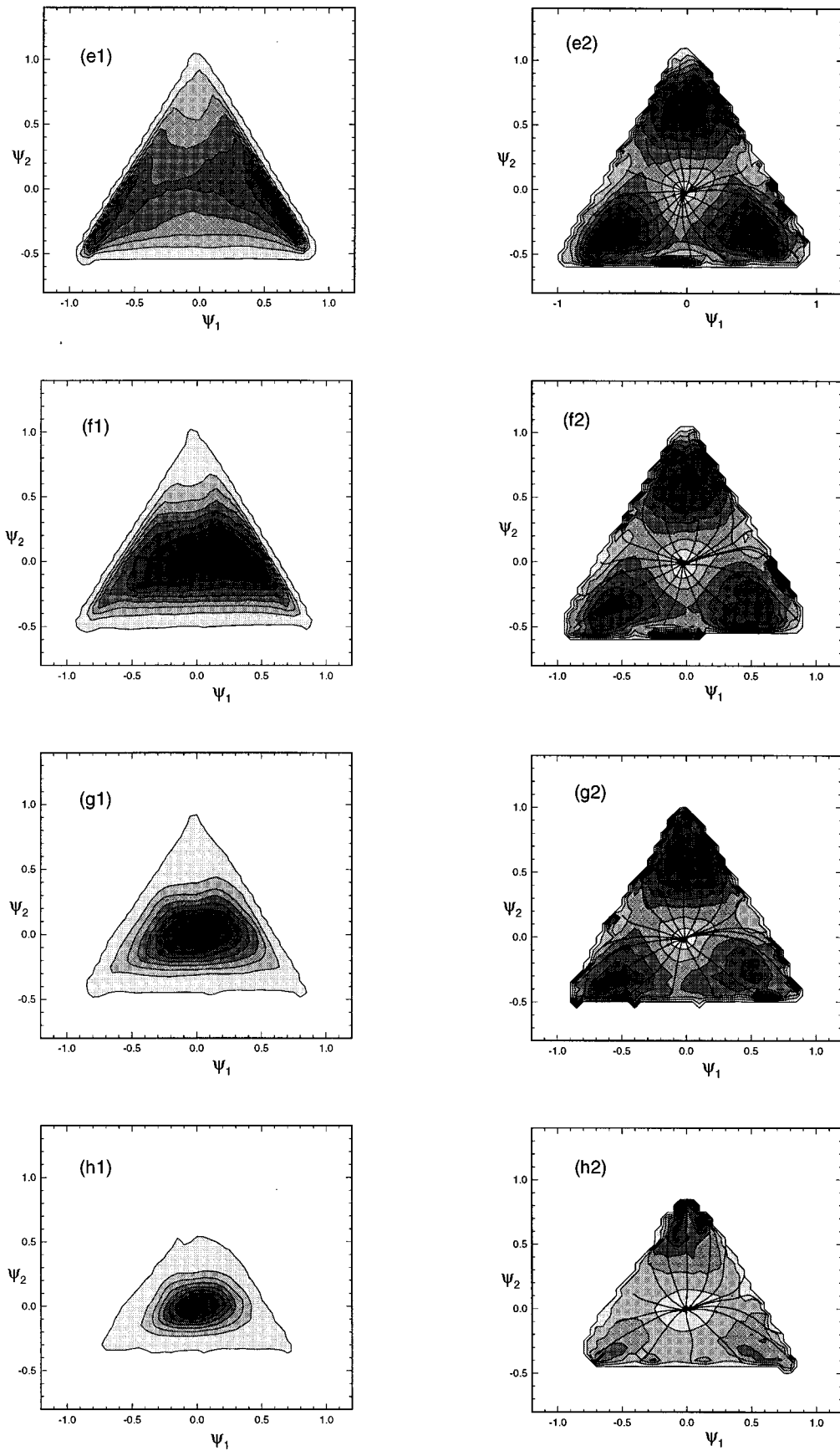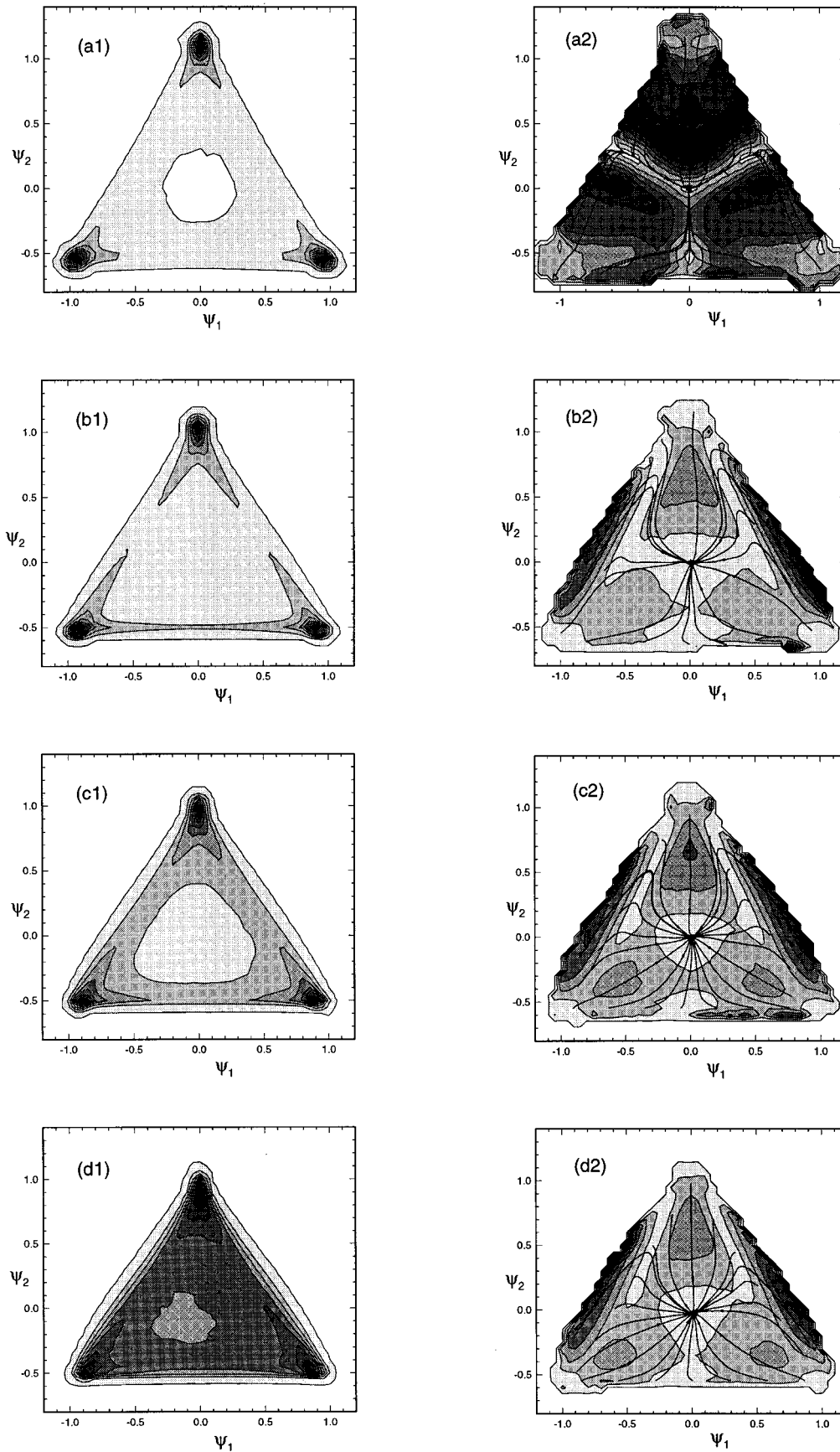
FIG. 8. Same as Fig. 4, but for R92E simulations.

Phys. Fluids, Vol. 8, No. 8, August 1996

A. Juneja and S. B. Pope   2175

FIG. 8. (*Continued.*)

A. Juneja and S. B. Pope
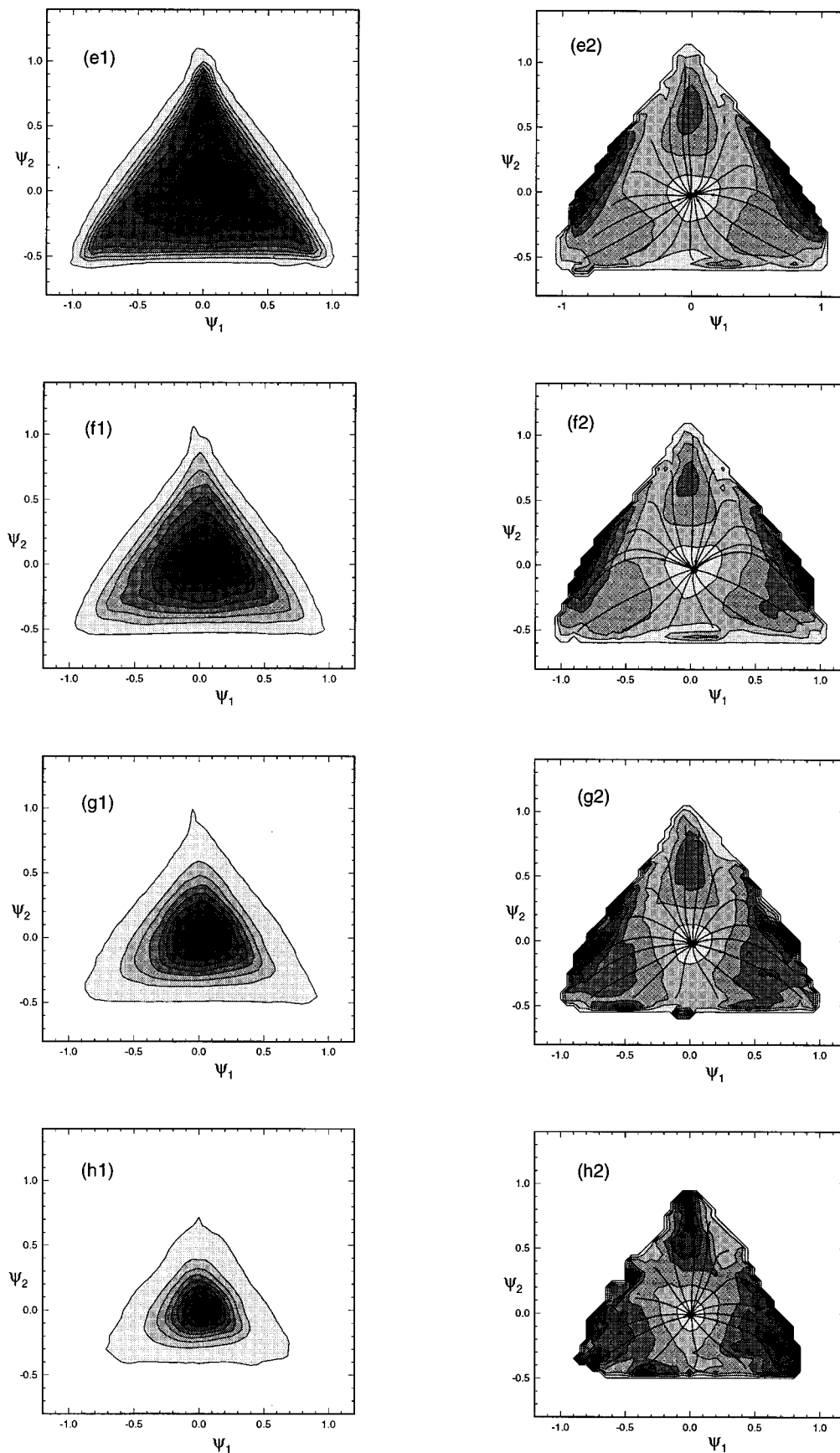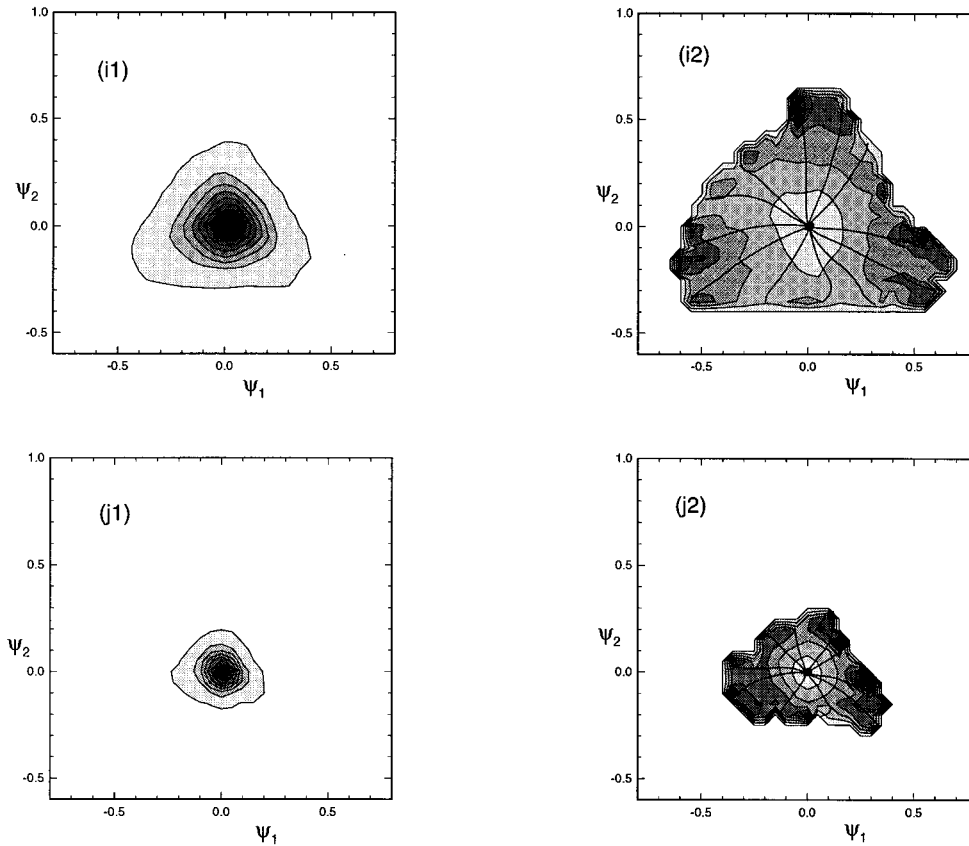
FIG. 8. (*Continued.*)

$$F(\mathbf{k}) = \begin{cases} 1, & \text{if } k \leq k_c, \\ (k/k_c)^{-2}, & \text{if } k > k_c, \end{cases} \tag{12}$$

k_c being the specified cutoff wavenumber. Therefore the second parameter in the specification of the initial scalar field is k_c/k_s. As explained in EP, it can be shown that beyond a value of k_c/k_s equal to 2, the effect of this parameter is not significant, as it only affects the smaller scales where the consequent variation is shortlived. Therefore we set the value of k_c to be twice the value of $(k_s)_{max}$, where $(k_s)_{max}$ refers to the k_s value of the scalar field with smaller initial length scale.

It is clear that the procedure described above allows the generation of two independent scalar fields whose initial length scales can be varied together or relative to one another. Hence this allows us to highlight the effect of initial length scales of the scalar fields on the mixing process. In addition, we also assess the effects of differential diffusion by varying the Prandtl number of one scalar relative to the other. Five different cases denoted by A, B, C, D and E are studied, which differ in the specified wavenumbers $(k_s/k_0)_1$ and $(k_s/k_0)_2$ used in the initialization, and the Prandtl numbers $Pr_{(\alpha)} \equiv \nu/D_{(\alpha)}$. These values are given in Table III. Also listed are the values of the covariance ($\langle \phi_1 \phi_2 \rangle$) and the integral length scales, l_{ϕ_α} for the initial scalar fields generated on a 192^3 grid, where

$$l_{\phi_\alpha} = \frac{1}{3} \sum_{i=1}^{3} \left(\frac{\pi}{2 \langle \phi_\alpha^2 \rangle} \right) E_{i\phi_\alpha}(0), \tag{13}$$

and $E_{i\phi_\alpha}(\mathbf{k})$ is the initial one-dimensional scalar-energy spectrum. Relative to the base case A, cases B and C have smaller and larger initial lengthscales, respectively. For these three cases the two scalars and the three initial states are statistically identical, and so the jpdf has six-way symmetry. Relative to the base case, in case D scalar 1 has approximately twice the initial lengthscale; while in case E, scalar 2 has twice the diffusivity (half the Prandtl number). In cases D and E the jpdf is symmetric about the ψ_2 axis. A contour plot of an arbitrary planar section through the scalar fields is shown in Fig. 2. It can be seen that the two scalars are predominantly in one of the three possible states with sharp gradients in between, thus conforming closely to a triple-delta function jpdf. The simulations presented in the next section are labeled according to the convention that R92B indicates a simulation of case B at $Re_\lambda = 92$, and so on.

IV. RESULTS

The primary focus of the current simulations is to study the evolution of the scalar jpdf and the conditional diffusion for the different initial scalar fields described in Table III. These results are presented in Sec. IV A. Other issues of

Phys. Fluids, Vol. 8, No. 8, August 1996
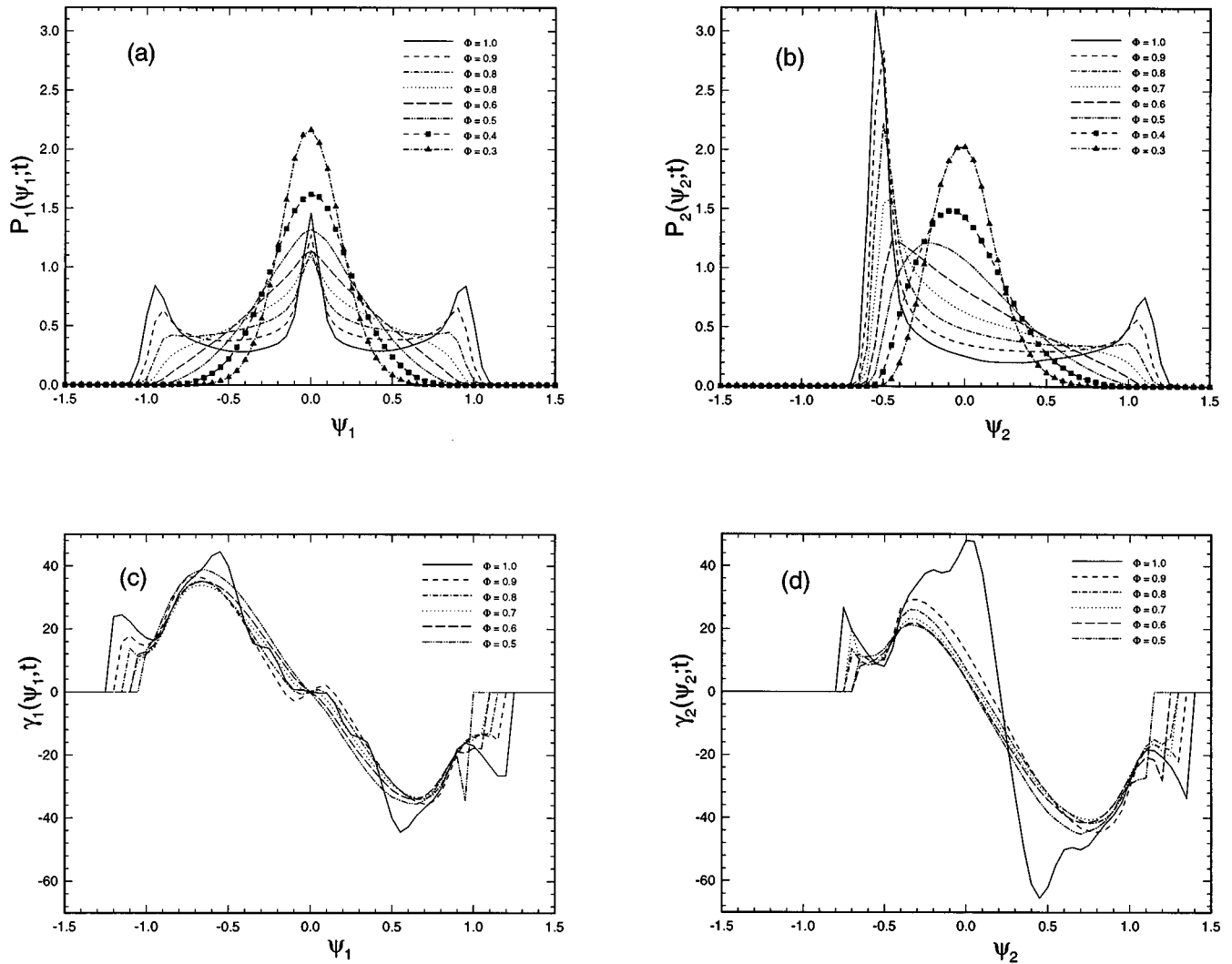
A. Juneja and S. B. Pope   2177

FIG. 9. The evolution states of the marginal pdf of (a) ϕ_1 and (b) ϕ_2 for simulation R92A. The corresponding conditional expectations of the scalar diffusion are shown in (c) for ϕ_1 and (d) for ϕ_2, respectively.

interest which are studied involve whether or not the scalar fields reach a self-similar state (Sec. IV B) and the rate of decay of the scalar variance and dissipation at large times (Sec. IV C). We shall present detailed results from the R92A simulations, where the initial length scales and the diffusivity for the two scalar fields are the same. For the other cases, we shall highlight the differences (if any) in the scalar mixing process caused by a change in either the initial length scale or the diffusivity. Except where noted, the results are from simulations utilizing the 192^3 grid at $Re_\lambda = 92$, i.e., R92.

It has been observed in some of the prior simulations (for example, EP) and experiments that for the mixing of a single scalar with varying initial length scales (but the same initial pdf), the evolution states of the scalar pdf are approximately invariant if they are computed at fixed values of ϕ'/ϕ_0'. Here ϕ' represents the root mean square (r.m.s.) value of the scalar at the given time and ϕ_0' is the r.m.s. value at time $t = 0$ (initial state), the r.m.s. values being computed by taking the square root of the volume averaged scalar variance. Hence in the present simulations, we output the

various statistics at fixed values of the r.m.s. $\Phi \equiv (\phi'/\phi_0')_1$ where the subscript 1 denotes that the ratio is computed for the first scalar. Figure 3 shows a plot of the evolution of the scalar r.m.s (ϕ') and volume averaged scalar dissipation $[\langle \epsilon_\phi \rangle \equiv D \langle \nabla \phi(x,t) . \nabla \phi(x,t) \rangle]$ from the R92A simulations. Time is normalized by the large eddy-turnover time, i.e. $t^* = tu/l$. It can be seen that, in this case where the initial length scales of the two scalars are identical, the evolution of ϕ' and $\langle \epsilon_\phi \rangle$ are also quite similar—the differences being entirely due to statistical variability.

A. Evolution of scalar jpdf and conditional diffusion

The scalar joint probability density function, $P(\psi,t)$, is computed at specified times t by dividing the ψ_1-ψ_2 sample space into 60×60 intervals and then forming a histogram using the values of the two scalars at each grid point. As there are about seven million grid points, the jpdf can be expected to have relatively small statistical errors. The jpdf is easily represented as a contour plot in the two-dimensional sample space.
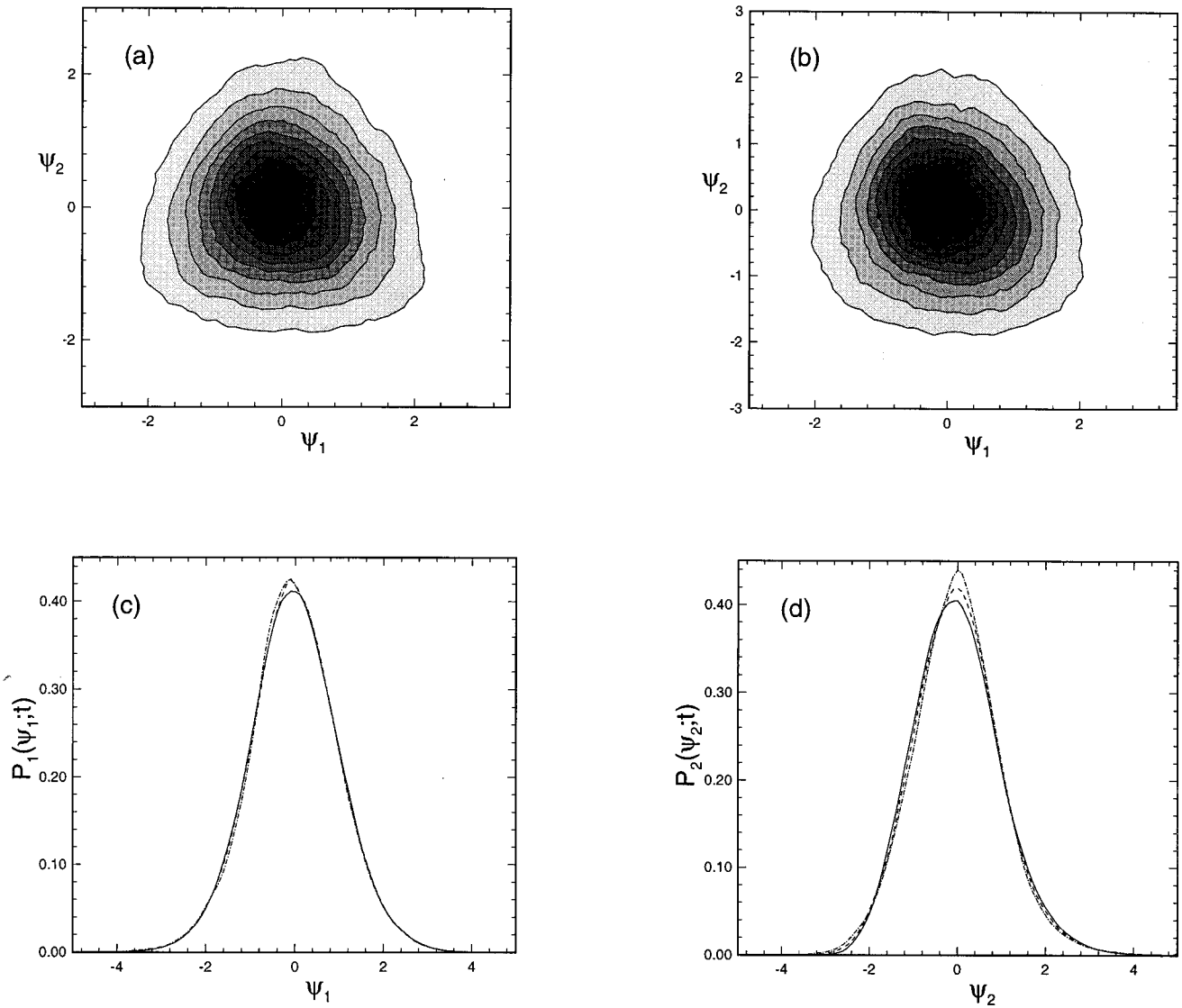
FIG. 10. The jpdf of the standardized scalar values at Φ equal to (a) 0.15 and (b) 0.1. The plots in (c) and (d) show the marginal pdf of the standardized values of the two scalars at $\Phi=0.2$, 0.15, and 0.1 (superposed lines) from simulation R92A.

As mentioned earlier, for homogeneous scalar fields in homogeneous turbulence, the primary quantity determining the evolution of the scalar jpdf is the expectation of the diffusion conditioned on the scalar value [see Eq. (2)]. This conditional expectation is estimated by generating a histogram of the scalar values weighted by the diffusion of each of the two scalars at the same point. The value of each component of this vector function is then divided by the unweighted histogram value of the scalar fields in the appropriate interval to yield the estimate of $\gamma(\psi,t)$. The conditional diffusion $\gamma_\alpha(\psi,t)=\langle D_{(\alpha)}\nabla^2\phi_\alpha|\phi(\mathbf{x},t)=\psi\rangle$ is the expected rate of change of ϕ_α, conditioned on $\phi=\psi$, and hence $\gamma=(\gamma_1,\gamma_2)$ corresponds to a ''velocity'' in composition space. The results are shown as contour plots of the ''speed'' $|\gamma|$ and of the ''streamlines,'' which are lines in the ψ_1-ψ_2 plane that are everywhere parallel to γ. The jpdf evolves by probability flowing along the ''streamlines'' at the ''speed'' $|\gamma|$.

Figure 4 shows the scalar jpdf and the conditional diffusion for the base case R92A simulations at r.m.s. $\Phi=1.0,0.9,0.8,0.7,0.6,0.5,0.4,0.3,0.2$ and 0.1, respectively. (Plate 1 shows the same plot in color at $\Phi=1.0,0.8,0.6$, and 0.4 along with contour plots of a planar slice through the initial scalar fields.) It may be seen from Figs. 4(a1)–4(d1) that at early times the jpdf evolves by probability flowing from the three delta functions along the lines joining them. This picture is confirmed by the streamline patterns on Figs. 4(a2)–4(d2). The streamlines accounting for the bulk of probability flow are nearly coincident with the sides of the triangle. Note that except for Fig. 4(a2) which is an artifact of the initial condition, the contour plot of the ''speed'' $|\gamma|$ has maxima along the three edges of the triangle; and that, by symmetry, there is a straight streamline from each delta function to the origin for all time. In physical space, it is the mixing across the initial interfaces between *pairs* of blobs

Phys. Fluids, Vol. 8, No. 8, August 1996
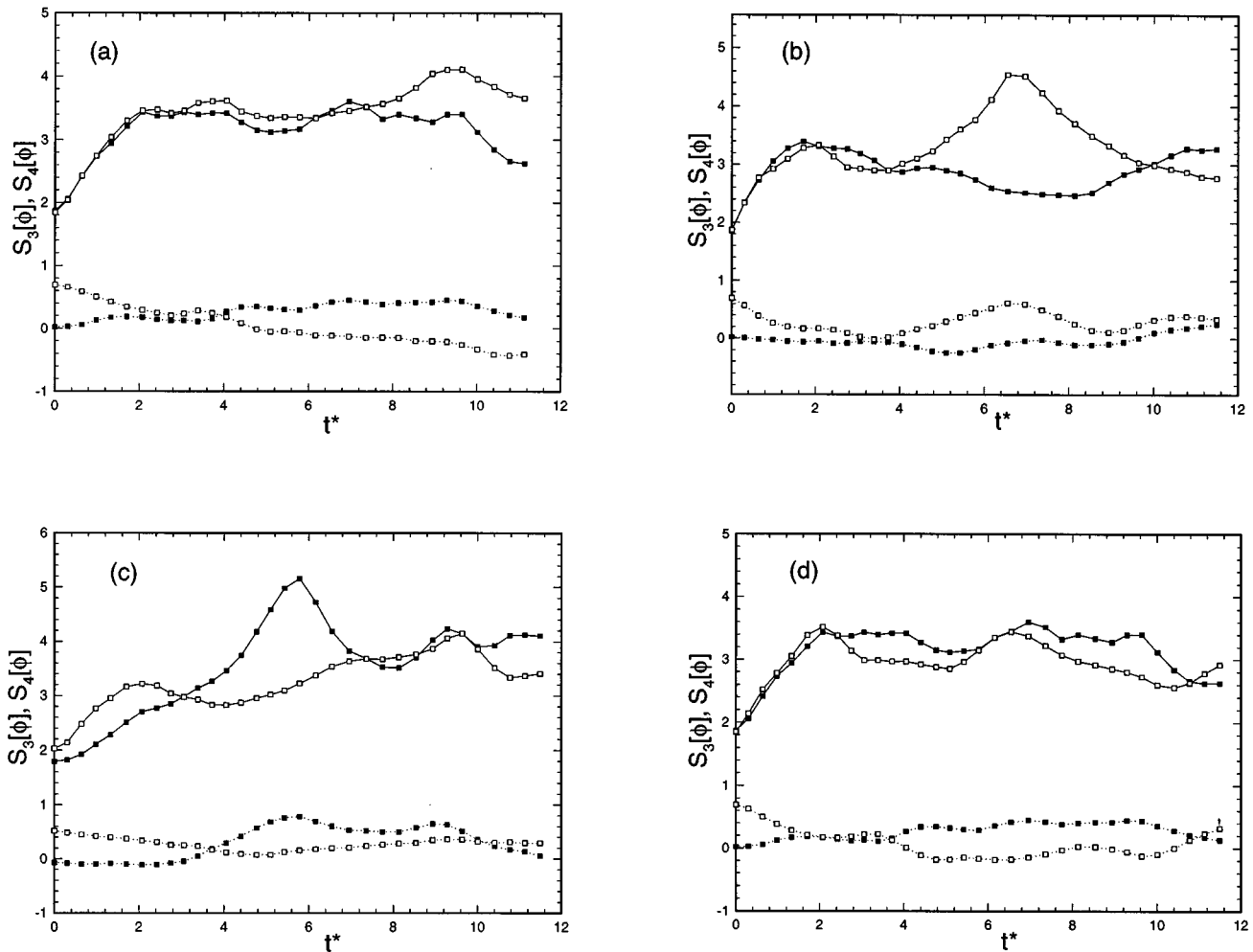
A. Juneja and S. B. Pope   2179

FIG. 11. The evolution of the skewness $[S_3(\phi)]$ (dashed lines) and the flatness $[S_4(\phi)]$ (solid lines) of the two scalars from (a) R48A, (b) R48B, (c) R48D, and (d) R48E simulations. Here and in subsequent plots, filled symbols are used for ϕ_1 and hollow symbols are used for ϕ_2.

that accounts for the triangular shape of the pdf at early times. It is worth noting that for a single-scalar case, a diffusive layer between $\phi_1 = -1.0$ and $\phi_1 = 1.0$ with an error function profile has a maxima of $|\nabla^2 \phi_1|$ at $\psi_1 = \pm 0.68$. This can be qualitatively observed in the contour plots in Figs. 4(b2)–4(d2) in the present case. As time evolves (e.g. $\Phi = 0.7$) the interior of the triangular jpdf fills in, and at $\Phi = 0.6$ the jpdf is remarkably uniform. Eswaran and Pope[1] also observed an approximately uniform pdf in the single-scalar case. Subsequently the peak of the jpdf is at the origin, and the triangular shape gradually changes to a circle at large times.

It is interesting to observe that if the jpdf decays as a joint normal distribution (as it approximately does for large times, $\Phi \lesssim 0.1$ say, see Sec. IV B), then the streamlines are radii, and the speed is linearly proportional to the distance from the origin. The simplest possible mixing model (IEM[22] or LMSE[23]) predicts this behavior at all times. Clearly, for the times shown in Fig. 4, both in direction and magnitude, the conditional diffusion is very different from this prediction. To provide a better guide for modeling efforts and to provide quantitative information on the evolution of condi-

tional diffusion, we plot the normalized value of its individual components in Fig. 5 along four lines in the ψ_1-ψ_2 plane as a function of time; the normalization of γ_1 and γ_2 is performed by dividing its value by $\epsilon_\phi/2\phi'$ for the first scalar at the given time.

Figure 6 shows the same plot as Fig. 4 from the R92B simulations. The evolution of the scalar jpdf and conditional diffusion look quite similar to Fig. 4 even though the initial length scales of the scalar fields B are different from those in A. We also carried out simulations employing the initial scalar field C ($k_s/k_0 = 2$ and $Pr = 0.7$ for both scalars). The plots (not shown here) are again very much like Figs. 4 and 6 and it can be concluded that, if the scalar initialization scheme described in Sec. III is employed, then as long as the initial length scales of the two scalars fields are the same relative to one another, it does not matter whether the value of the length scale itself is varied between simulations, if one is interested in the evolution states of the scalar jpdf and conditional diffusion at fixed values of Φ.

In order to assess the effect of varying the initial length scales of the scalar fields relative to one another, we next
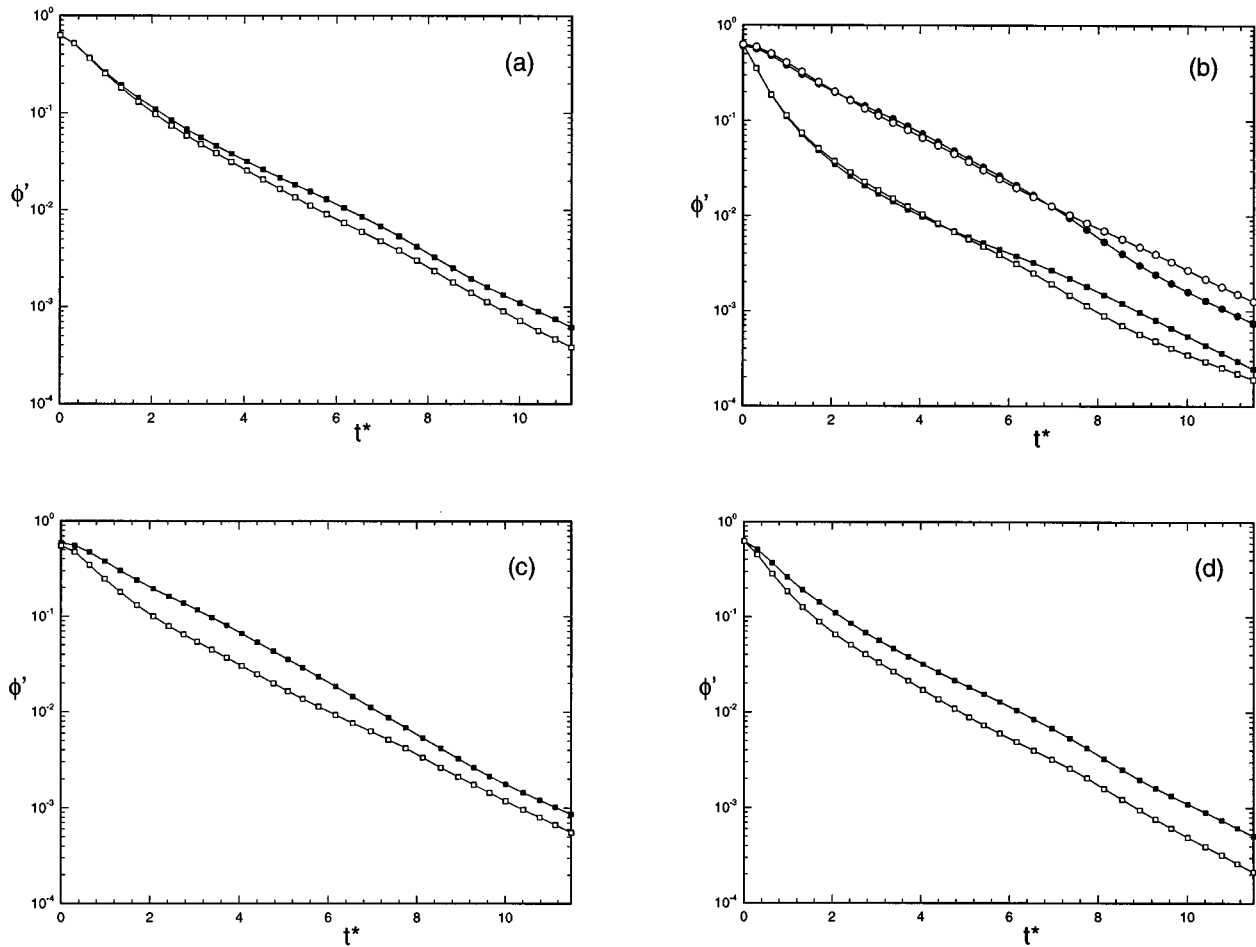
A. Juneja and S. B. Pope

FIG. 12. The decay of the scalar r.m.s. values from (a) R48A, (b) R48B (squares) and R48C (circles), (c) R48D, and (d) R48E simulations.

present the results from R92D simulations employing the initial scalar field D in which $(k_s/k_0)_1 = 2$ and $(k_s/k_0)_2 = 4$ while $Pr = 0.7$ for both scalars. Figure 7 shows the evolution of the scalar jpdf and the conditional diffusion for this case. It is seen that the mixing is faster in the ψ_2 direction. This is to be expected as the scalar with a smaller initial length scale tends to mix more rapidly. In this case, the jpdf spreads much more slowly along the edge of the triangle aligned with the ψ_1 axis when compared to the other two edges of the triangle. Again the trend is explained by looking at the the plots for the conditional diffusion. Most of the streamlines indicate a faster initial mixing along the ψ_2 axis which dictates the evolution of the scalar jpdf.

If, on the other hand, the diffusivity of the second scalar is set to twice the value of that for the first scalar while keeping the initial length scales to be the same (scalar field E), a similar albeit much less pronounced effect on the evolution of the jpdf can be observed (Fig. 8[16]). The second scalar again tends to mix a little faster than the first scalar and this causes the edge of the triangle parallel to the ψ_1 axis to bend more towards the origin near the center than the other two edges. The resulting concave shape of the edge of parallel to the ψ_1 axis and the convex nature of the other two edges is best seen in Figs. 8(c1) and 8(d1). It is worth noting that the increase in diffusivity causes the scalar jpdf at early

times to stretch outside the triangle described by the initial state jpdf, unlike the previous cases. Once again, the jpdf has a somewhat flat distribution at $\Phi = 0.6$, before it begins to lose its triangular shape. The corresponding plots for the conditional diffusion show much more clearly the effect of changed diffusivity, when compared to those for scalars with equal diffusivity and equal length scales. It is also useful to note that changing the length scale and the diffusivity of the scalars are two completely different issues even though their effects in the present case are somewhat similar. The effect due to the change in length scale is expected to be present even as the Reynolds number goes to infinity, whereas the effect due to increased diffusivity should gradually disappear as the Reynolds number is increased.

We also independently computed the marginal pdf's of the two scalars, $P_1(\psi_1,t)$ and $P_2(\psi_2,t)$ and the conditional expectation of diffusion for the individual scalars $[\gamma_1(\psi_1,t) = \langle \nabla^2 \phi_1 | \phi_1 = \psi_1 \rangle$ and $\gamma_2(\psi_2,t) = \langle \nabla^2 \phi_2 | \phi_2 = \psi_2 \rangle]$ by forming histograms using 100 sampling intervals. Figure 9 shows the respective plots from the R92A simulations. It can be observed from Figs. 9(a) and 9(b) that, even though the initial shape for the marginal pdf's for the two scalar are quite different from one another, they assume a similar near-Gaussian shape by the time $\Phi = 0.3$. Also, the plots of the individual conditional scalar diffusion

Phys. Fluids, Vol. 8, No. 8, August 1996
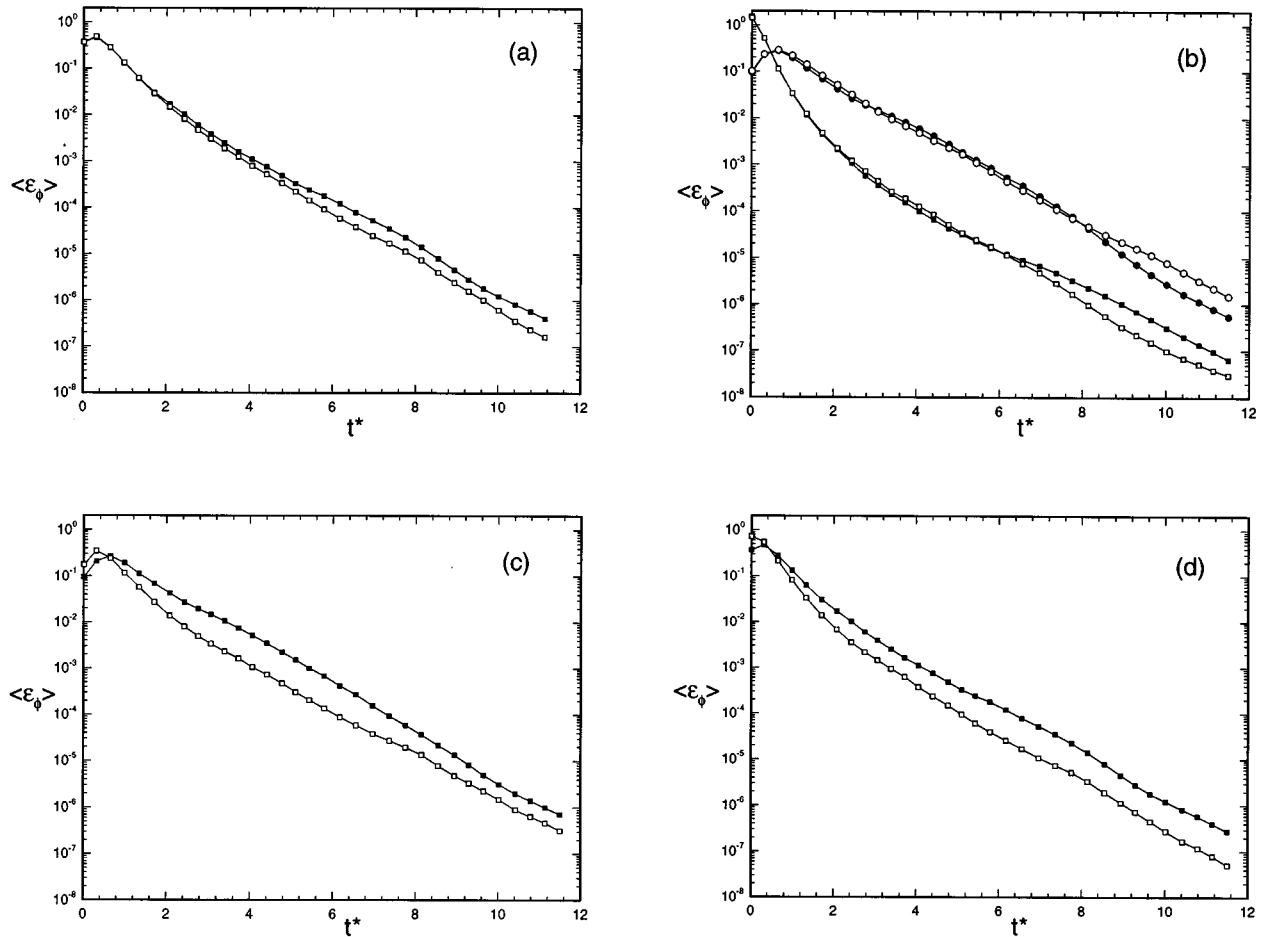
A. Juneja and S. B. Pope   2181

FIG. 13. The evolution of the scalar dissipation rate from (a) R48A, (b) R48B (squares) and R48C (circles), (c) R48D, and (d) R48E simulations.

indicate a linear region in the center at larger times (i.e., smaller values of Φ), as has been observed before both numerically and experimentally. As a final remark, we examined the evolution of the scalar jpdf and conditional diffusion on the smaller 96^3 grid at a Taylor scale Reynolds number of $Re_\lambda = 48$. The results look very similar and this suggests that the mixing process is not strongly influenced (at least qualitatively) by the Reynolds number in the range considered.

B. Self-similarity at later times

Next, we address the issue of the self-similarity of the scalar fields at larger times. This is done by examining the standardized joint and the marginal pdf's of the two scalars - i.e., the pdf's of the two scalars normalized by their respective r.m.s. values at the given time. The plots of the standardized jpdf's at $\Phi = 0.15$ and 0.1 are shown in Figs. 10(a) and 10(b). These results have been extracted from the R92A simulations. The shapes of the two jpdf's are quite similar, and in general it was found that the standardized jpdf's have a statistically self-similar shape which is close to a joint-normal for $\Phi \leq 0.25$. It should however be noted that for cases D and E, this jpdf has different variances for the two scalars at all times, i.e. ϕ_1' is greater than ϕ_2' (see Fig. 12). The plot of the standardized marginal pdf's of the two scalars

(once again normalized by the respective r.m.s. values) at three different values of Φ equal to 0.20, 0.15, and 0.1 are shown superimposed on each other in Figs. 10(c) and 10(d). The different curves seem to lie on top of each other indicating that a self-similar state has been reached.

Another way of examining the self-similar state of a pdf is to plot the value of the normalized moments of the pdf as a function of the time. Since this self-similarity will be evident only at larger times, we ran simulations for about twelve large-eddy turnover times, but on a smaller 96^3 grid in order to keep computational costs low. Figure 11 shows the evolution of the normalized third and fourth moments (skewness and flatness respectively) of the marginal scalar pdfs. (Here $S_m[q]$ denotes the mth normalized central moment of the random variable q.) It is seen that at the initial time, the first scalar has zero skewness and the second scalar has a positive skewness of around 0.75 while the flatness for both is close to 1.8 in all cases. As the simulation progresses, the second scalar loses its positive skewness, and after a while the skewness of both scalars is found to oscillate around zero, whereas the flatness initially rises and then fluctuates around a value close to 3.5 independently of the choice of the initial scalar fields employed in the simulations. (The statistical
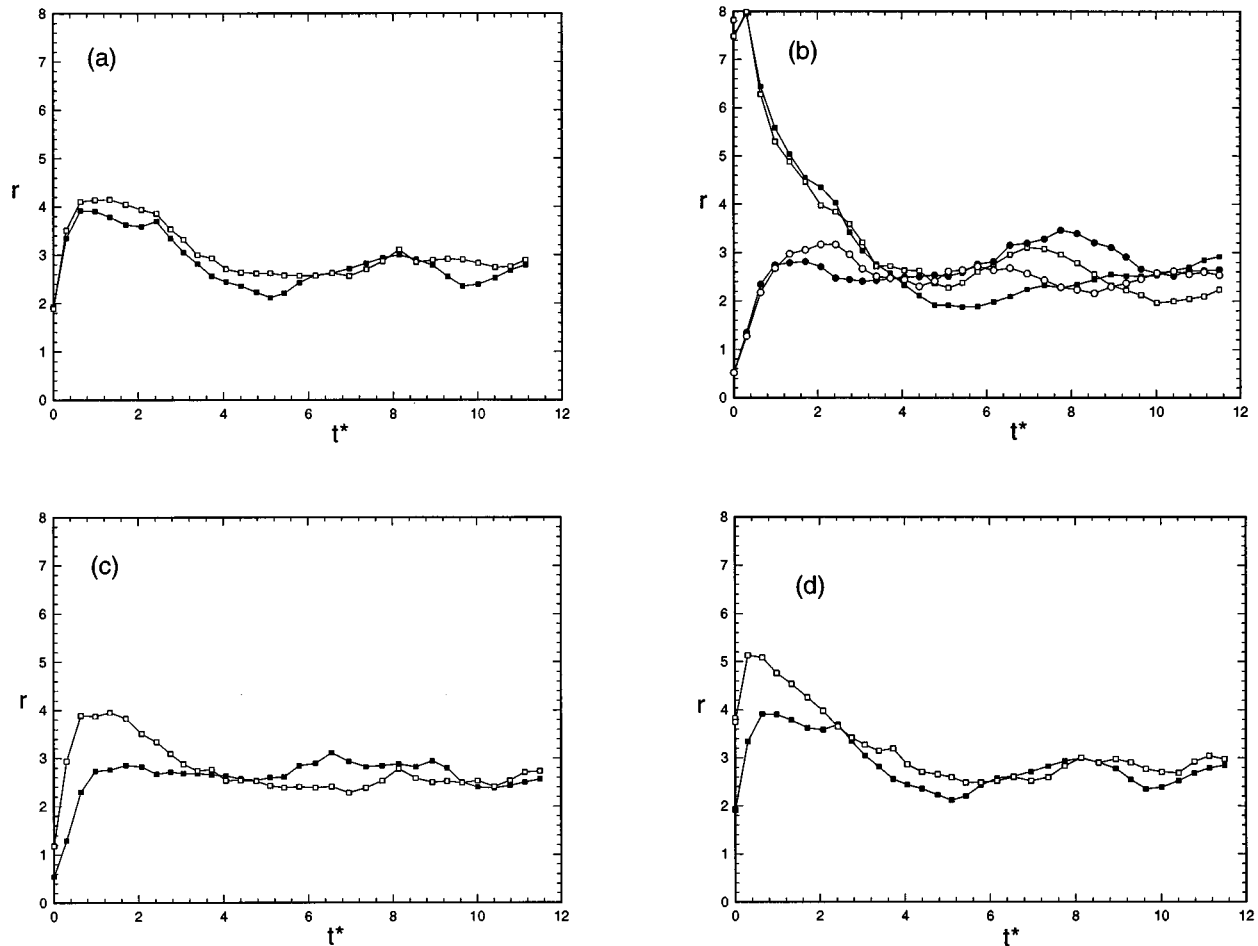
A. Juneja and S. B. Pope

FIG. 14. The evolution of the mechanical-to-scalar time-scale ratio r from (a) R48A, (b) R48B (squares) and R48C (circles), (c) R48D, and (d) R48E simulations.

C. Evolution of scalar variance and dissipation

In the case of a single scalar with a specified initial pdf, the initial decay rate of the scalar variance and dissipation is known to depend on the initial length scale of the scalar.[24] However, at large times, these decay rates may become similar (in stationary turbulence)[1,25] leading to a universal value of the mechanical-to-scalar time-scale ratio defined by $r \equiv (\langle \epsilon_\phi \rangle / \langle \phi^2 \rangle)/[\epsilon/(3u^2)]$. Hence it is of interest to investigate the decay rates for the present problem where the marginal pdf's of the two scalars are also significantly different from one another. Again, the results are extracted from the simulations performed on the smaller 96^3 grid at $Re_\lambda = 48$ to facilitate longer runs. The decay of the r.m.s. values of the two scalars for different initial scalar fields is plotted in Fig. 12. It is seen that for initial scalar fields A, B, C [Figs. 12(a) and 12(b)], where the length scales of the two scalars are equal relative to one another, the initial rate of decay of ϕ'_1 and ϕ'_2 is almost indistinguishable. At large times, there seems to be some difference in the decay rate but we can attribute that to statistical variability (see Fig. 8 in EP). In

case of simulations employing different initial length scales for the scalars (D) or different diffusivities (E), it is seen that the scalar with the smaller initial length scale [Fig. 12(c)] or higher diffusivity [Fig. 12(d)] decays faster, at least initially, than the other scalar. Similar trends are observed in the evolution of the mean scalar dissipation rate $\langle \epsilon_\phi \rangle$ as shown in Fig. 13. In Fig. 14 we plot the evolution of the time-scale ratio r with time. It was found in EP that for the case with one scalar, this ratio r evolves to a universal value in the vicinity of 2.5 independent of the initial length scale. This observation is also confirmed by the current simulations as r seems to relax to a universal value between 2 and 3 for the different initial scalar fields employed in the present work.

V. CONCLUSIONS

We have studied the mixing of two passive scalars in stationary, homogeneous, isotropic turbulence using direct numerical simulations on a 192^3 grid at a Taylor-scale Reynolds number of $Re_\lambda = 92$. The initial scalar fields are chosen to conform closely to a ''triple-delta function'' jpdf corresponding to blobs of fluids in three distinct states. We study the effect of initial length scales and diffusivity of the scalars on the mixing process, as the scalars are allowed to decay

Phys. Fluids, Vol. 8, No. 8, August 1996

A. Juneja and S. B. Pope   2183

from their prescribed initial state. In all the cases considered, the scalar jpdf initially tends to spread mainly along the edges of the triangle formed by the three delta functions. In physical space this corresponds to the mixing between adjacent pairs of blobs. Further, the decay of the scalar fields causes the triangle to shrink slowly towards the origin. When plotted at fixed values of the r.m.s. Φ, the evolution states of the jpdf do not depend on the initial length scale of the scalars, as long as they are the same for both. The effect of changing the length scale or diffusivity of one scalar relative to the other manifests itself in the form of faster mixing in the direction of the scalar with the smaller length scale or the higher diffusivity, respectively. Another notable feature is that the scalar jpdf assumes a relatively flat triangular distribution, before it loses the inherited triangular shape from the initial state and starts evolving to a near joint-normal form. These trends in the evolution of the jpdf are explained by examining the corresponding plots for the conditional scalar diffusion, which can be used to formulate better mixing models for the multi-scalar case.

ACKNOWLEDGMENTS

[1] V. Eswaran and S. B. Pope, ''Direct numerical simulations of the turbulent mixing of a passive scalar,'' Phys. Fluids **31**, 506 (1988).

[2] K. R. Sreenivasan, S. Tavoularis, R. Henry, and S. Corrsin, ''Temperature fluctuations and scales in grid-generated turbulence,'' J. Fluid Mech. **100**, 597 (1980).

[3] Jayesh and Z. Warhaft, ''Probability distributions, conditional dissipation, and transport of passive temperature fluctuations in grid-generated turbulence,'' Phys. Fluids A **4**, 2292 (1992).

[4] P. E. Dimotakis, R. C. M. Lye, and D. A. Papantoniou, ''Structure and dynamics of round turbulent jets,'' Phys. Fluids **28**, 3185 (1983).

[5] R. R. Prasad and K. R. Sreenivasan, ''Quantitative three-dimensional imaging and the structure of passive scalar fields in fully turbulent flows,'' J. Fluid Mech. **216**, 1 (1990).

[6] W. J. A. Dahm, K. B. Sutherland, and K. A. Buch, ''Direct high-resolution 4-dimensional measurements of the fine scale structure of Sc greater-than 1 molecular mixing in turbulent flows,'' Phys. Fluids A **3**, 1115 (1991).

[7] R. M. Kerr, ''Higher-order derivative correlations and alignment of small-scale structures in isotropic numerical turbulence,'' J. Fluid Mech. **153**, 31 (1985).

[8] G. A. Blaisdell, N. N. Mansour, and W. C. Reynolds, ''Compressibility effects on the passive scalar flux within homogeneous turbulence,'' Phys. Fluids **6**, 3498 (1994).

[9] A. Pumir, ''A numerical study of the mixing of a passive scalar in three dimensions in the presence of a mean gradient,'' Phys. Fluids **6**, 2118 (1994).

[10] J. R. Chasnov, ''Similarity states of passive scalar transport in buoyancy-generated turbulence,'' Phys. Fluids **7**, 1498 (1995); ''Similarity states of passive scalar transport in isotropic turbulence,'' **6**, 1036 (1994).

[11] S. B. Pope, ''PDF methods for turbulent reactive flows,'' Prog. Energy Combust. Sci. **11**, 119 (1985).

[12] S. B. Pope, ''Mapping closures for turbulent mixing and reaction,'' Theo. Comput. Fluid Dyn. **2**, 255 (1991).

[13] A. R. Kerstein, ''Linear-Eddy modeling of turbulent transport: Part II. Application to shear layer mixing,'' Combust. Flame **75**, 397 (1989).

[14] A. Sirivat and Z. Warhaft, ''The mixing of passive helium and temperature fluctuations in grid turbulence,'' J. Fluid Mech. **120**, 475 (1982).

[15] Z. Warhaft, ''The use of dual heat injection to infer scalar covariance decay in grid turbulence'' J. Fluid Mech. **104**, 93 (1981).

[16] P. K. Yeung and S. B. Pope, ''Differential diffusion of passive scalars in isotropic turbulence,'' Phys. Fluids A **5**, 2467 (1993).

[17] J. R. Saylor, ''Differential diffusion in turbulent and oscillatory nonturbulent water flows,'' PhD thesis, Yale University, 1993.

[18] R. S. Rogallo, ''Numerical experiments in homogeneous turbulence,'' NASA TM-81315, 1981.

[19] V. Eswaran and S. B. Pope, ''An examination of forcing in direct numerical simulations of turbulence,'' Comput. Fluids **16**, 257 (1988).

[20] P. K. Yeung and S. B. Pope, ''Lagrangian Statistics from direct numerical simulations of isotropic turbulence,'' J. Fluid Mech. **207**, 531 (1989).

[21] P. K. Yeung and C. A. Moseley, ''A message-passing, distributed memory parallel algorithm for direct numerical simulation of turbulence with particle tracking,'' in *Parallel Computational Fluid Dynamics: Implementation and Results Using Parallel Computers*, edited by A. Ecer, J. Periaux, N. Satofuka and S. Taylor (Elsevier Science, New York, 1995).

[22] J. Villermaux and J. C. Devillon, in *Proceedings of the 2nd International Symposium on Chemical Reaction Engineering* (Elsevier Science, New York, 1972).

[23] C. Dopazo and E. E. O'Brien, ''An approach to the autoignition of a turbulent mixture,'' Acta Astronaut. **1**, 1239 (1974).

[24] Z. Warhaft and J. L. Lumley, ''An experimental study of the decay of temperature fluctuations in grid generated turbulence,'' J. Fluid Mech. **88**, 659 (1978).

[25] P. A. Durbin, ''Analysis of the decay of temperature fluctuations in isotropic turbulence,'' Phys. Fluids **25**, 1328 (1982).

A. Juneja and S. B. Pope